ACS OMEGA

http://pubs.acs.org/journal/acsodf

Article

Pore Structure and Adsorption Characteristics of Maceral Groups: Insights from Centrifugal Flotation Experiment of Coals

TengFei Jia, Songhang Zhang,* Shuheng Tang, Di Xin, Qian Zhang, and Ke Zhang

Cite This: *ACS Omega* 2023, 8, 12079−12097

Read Online

ACCESS | Metrics & More | Article Recommendations

ABSTRACT: Coal has various types of macerals, which have different pore structures and adsorption properties that change with coal's thermal metamorphism. In-depth study of the characteristics of different coal macerals, especially the pore structure and adsorption properties, can better predict the coal reservoir gas storage capacity and migration ability. In this study, the sub-samples enriched in a specific maceral group with different coal ranks and particle sizes were obtained by centrifugal flotation experiments. Then, experiments containing low-temperature N_2 isotherm adsorption (LT-N_2GA), low-temperature CO_2 isotherm adsorption (LT-CO_2GA), and methane isothermal adsorption were carried out on the sub-samples to quantitatively analyze the evolution characteristics of pore structure and adsorption properties of different maceral groups. The results showed the following: (1) The separation effect of the light maceral groups by centrifugal flotation experiments increased with the decrease of particle sizes, which were treated with the heavy liquid of low and medium densities, while that of the heavy maceral groups had the relatively best separation effect in the particle sizes of 0.1−0.125 mm, which were treated with the heavy liquid of high densities. (2) The vitrinite-enriched samples had more ultra-micropores (mainly within the diameter range of 0.4−0.65 nm), while the inertinite enriched samples had more mesopores and transition pores (mainly within the diameter range of 40−50 nm). (3) For the low-rank coal, inertinite had more potential methane adsorption capacity. However, for the medium- and high-rank coal, vitrinite had more potential methane adsorption capacity. (4) For the low-rank coal, the adsorption potential and adsorption space increased with the increase of the inertinite content, while the adsorption potential, adsorption space, and surface free energy for the medium- and high-rank coal increased with the increase of vitrinite content. It is expected that the results can deepen the understanding about the gas storage capacity and migration ability and be used in the prevention of gas outburst and the reduction of carbon emission.

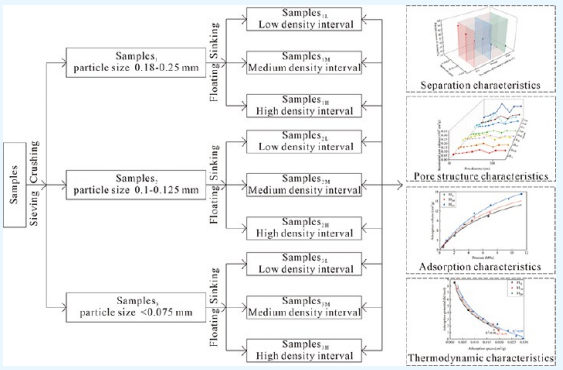

1. INTRODUCTION

In recent years, all kinds of environmental problems caused by the greenhouse effect have emerged frequently.[1,2] Countries around the world are actively responding to them and putting forward measures, such as carbon capture, utilization, and storage (CCUS),[3,4] to reduce global carbon emissions.[5,6] CO_2 geological sequestration can be stored into brine aquifers, deep ocean, depleted oil and gas reservoirs, deep coal seams, and so on. Among the carbon dioxide storage sites, deep coal seams are regarded as one of the potential sites.[7,8] Carbon sequestration in coal seam can improve coalbed methane (CBM) recovery,[9] prevent coal mine gas outburst accidents,[10−12] and further realize the strategic planning of net-zero carbon emission,[13,14] which has been paid more and more attention. The storage of carbon dioxide in coal, the development of CBM, and coal mine gas outburst accidents are all related to the adsorption characteristics of coal.[15−18] At present, the adsorption characteristics of coal on gas, such as carbon dioxide, methane, nitrogen, and flue gas, have been deeply studied and the related results can be divided into two main categories. The first category mainly focuses on the influence of the properties of coal on gas adsorption, such as pore structure[19] and maceral groups.[20] The second category mainly focuses on the influence of external conditions on gas adsorption, such as temperature[21] and particle size.[22]

There is a consistent understanding of the influence of external factors on the adsorption of coal, but there is still a dispute on the influence of coal maceral groups. Most scholars found that the gas adsorption capacity of vitrinite was stronger than that of inertinite,[23−29] while a few scholars found that the gas adsorption capacity of inertinite was stronger than that of vitrinite,[30−33] and some other scholars found that there was no

Received: December 15, 2022
Accepted: March 9, 2023
Published: March 21, 2023

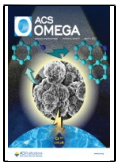

https://doi.org/10.1021/acsomega.2c07876
ACS Omega 2023, 8, 12079−12097

Table 1. Results of $R_{o,max}$, Maceral Composition, and Proximate Analysis of the Samples[a]

			maceral composition (vol %)				proximate analysis (vol %)			
coal mine	coal type	$R_{o,max}$ (vol %)	V/H	L	I	M	M_{ad}	A_d	V_d	FC_d
Hequ	long flame coal	0.56	50.3	1.4	39.9	8.4	3.09	22.04	28.95	49.01
Rongtai	coking coal	1.70	47.2	/	48.9	3.9	0.91	10.14	16.50	73.36
Zhaozhuang	meager coal	2.21	57.8	/	36.0	6.2	0.76	10.11	9.39	80.50

[a]V: vitrinite content, vol %; H: huminite content, vol %; L: liptinite content, vol %; I: inertinite content, vol %; M: mineral content, vol %; M_{ad}: moisture content (air-dried basis), vol %; A_d: ash yield (dry basis), vol %; V_d: volatile content (dry basis), vol %; FC_d: fixed carbon content (dry basis), vol %.

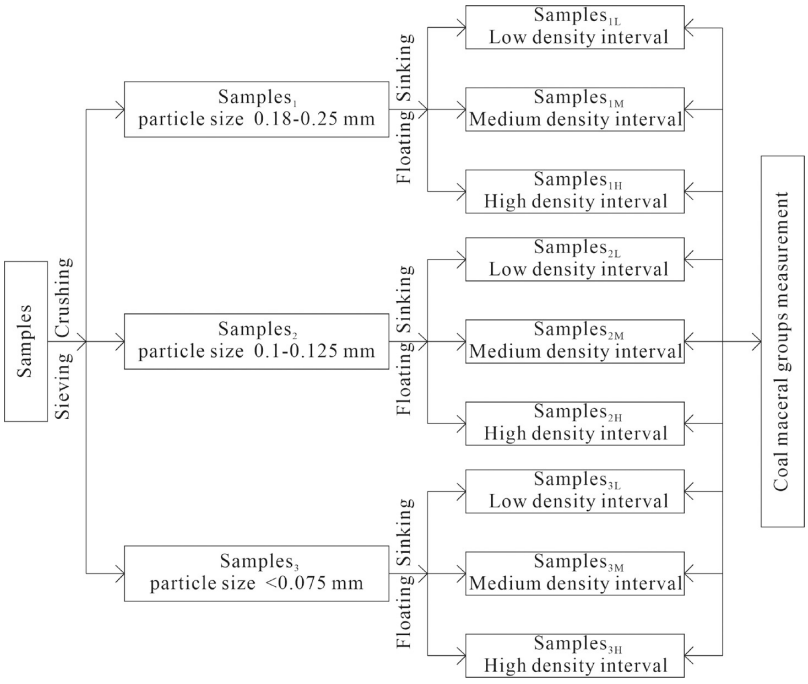

Figure 1. Schematic of the experimental process for the separation of maceral groups of samples.

obvious relationship between vitrinite and inertinite and gas adsorption capacity.[34−38]

Because most of the gas adsorption on coal is physical adsorption, the difference of maceral groups' adsorption performance is mainly controlled by the difference of pore structure.[39,40] Corresponding with the understanding of the adsorption properties of coal macerals, there are also different views on the development of pore structure of coal macerals. Shan et al.[41] found that pores <0.64 nm were more developed in inertinite-rich coals, while Zhang and Fu[42] found that pores <2 nm were more developed in vitrinite-rich coals. Generally, the reason for the different conclusions is mostly related to the heterogeneity of coal and the different contrast criteria, such as coal rank, coal maceral, and mineral content. The centrifugal flotation experiment of coal, which can obtain samples with the same coal rank and different maceral groups, provides a basis for accurate analysis of the pore structure and adsorption properties of macerals.

The adsorption of gas by coal is essentially the interaction between solid molecules and gas molecules.[40] The process of adsorption equilibrium is often accompanied by changes in energy, and the coal surface always tends to reduce the energy to adsorb gas molecules to a stable state.[43,44] From the view of thermodynamic properties, the characteristics of adsorption potential, adsorption space, and surface free energy can satisfactorily characterize the adsorption capacity of coal for gas.[44,45] At present, a lot of work has been carried out on the thermodynamic properties of methane adsorption by coal.[46−51] Lu et al.[50] found that the stronger the tectonic deformation, the greater the reduction of surface free energy and the higher the amount of methane adsorbed. Zhang et al.[51] found that high-rank coal samples had higher adsorption space, adsorption potential, and methane adsorption capacity than the medium-rank coal samples. However, few literatures have reported the thermodynamic properties of methane adsorption by maceral groups.

Because the study of pore structure and adsorption capacity of coal macerals can more accurately predict the carbon dioxide storage capacity of coal reservoirs, the CBM content and production characteristic, and the coal mine gas outburst potential,[7,9,52] it is necessary to study the pore and adsorption properties of coal maceral groups, so as to achieve the purpose of greenhouse gas control, carbon emission reduction, and gas outburst accident.[13,14] In addition, despite that a large number of studies about the pore structure of coal have been published, little is known about how the maceral groups of different coal ranks and particle sizes affect the distribution of pore structure and the thermodynamic properties.

On the basis of this fact, the low-, medium-, and high-rank coal samples with different particle sizes were prepared in this study. The sub-samples concentrated with different contents of vitrinite or inertinite were obtained using centrifugal flotation

https://doi.org/10.1021/acsomega.2c07876
ACS Omega 2023, 8, 12079−12097

Figure 2. Pulverized coal and coal bricks after separation (R, a: pulverized coals; b: coal bricks).

experiments. Meanwhile, the influence of particle size on the separation of maceral groups was determined. The pore structure characteristics, methane adsorption capacity, and thermodynamic properties of the separated samples were studied using LT-N_2GA, LT-CO_2GA, and methane isothermal adsorption experiments. Finally, the evolution characteristics of different maceral groups in various coal ranks were determined. This study not only contributes to a deeper understanding of the evolution characteristics and adsorption capacities of different maceral groups but also brings a better prospect for carbon sequestration.

2. EXPERIMENTAL SECTION

2.1. Sample Selection. In this study, the samples were taken from the Hequ (H), Rongtai (R), and Zhaozhuang (Z) coal mines. The Hequ and Rongtai coal mines are located on the eastern margin of Ordos Basin, whereas the Zhaozhuang coal mine is in the south of Qinshui Basin in China. All collected samples were immediately wrapped with polyethylene film to prevent the oxidation and sent directly to the laboratory. The results of maceral compositions, proximate analysis, and the maximum reflectance of vitrinite ($R_{o,max}$) of samples are listed in Table 1. During the experiments, China National Standards GB/T 8899-2008, GB/T 212−2008, and GB/T 6948−2013 were followed to achieve standardized experimental operations.

2.2. Methods. *2.2.1. Methodology of the Centrifugal Flotation.* The centrifugal flotation method separates maceral groups based upon their differences in densities. The brief experimental process and the scheme for naming the samples are shown in Figure 1. The centrifugal flotation experiments were carried out using the HITACHI-20PR-52D automatic centrifuge following the Chinese National Standard of GB/T 478-2008. The practical steps are as follows. (1) All the samples were first crushed into powder. The powdered samples with the particle sizes of 60−80 (0.18−0.25 mm), 120−150 (0.1−0.125 mm), and >200 (<0.075 mm) mesh were obtained by sieving. Meanwhile, the powdered samples were sealed into a vacuum glass bottle. (2) Next, aqueous $ZnCl_2$ solution with densities of 1.34 and 1.39 g/cm^3 for low-rank coal samples, 1.25 and 1.4 g/cm^3 for medium-rank coal samples, and 1.4 and 1.45 g/cm^3 for high-rank coal samples were prepared. The density errors were controlled to less than 0.005 g/cm^3. (3) Then, 100 g of low-rank coal powdered samples (60−80 mesh) was taken in a beaker and an appropriate amount of heavy liquid with the density of 1.34 g/cm^3 was added to the beaker. The beaker was placed in a blender and stirred for 20 min. (4) The mixture was placed in a centrifugal bottle for centrifugation. The rotational speed of the centrifuge was 2500 rpm, while the centrifugation time was 20−30 min. (5) After the centrifuge stopped working, the centrifugal bottle was removed and stood still for 2 h. (6) The powdered samples floating on top of the heavy liquid were collected. The collected samples were put into a Buchner funnel, washed with distilled water, and filtered. The low-rank wet powder samples of low density were obtained. (7) The samples sunk at the bottom of the bottle were collected. Steps 3−6 were repeated using a heavy liquid with a density of 1.39 g/cm^3 to obtain low-rank coal samples of medium density and high density. (8) Steps 2−7 were repeated to obtain the low-, medium-, and high-density powdered samples for low-, medium-, and high-rank coal samples with different powder sizes, respectively (Figure 2a). (9) The wet samples were dried in a vacuum oven for 12 h at a temperature of 378.15 K to prepare them for pore structure and isotherm adsorption experiments. In addition, coal bricks were made for microscopic analysis (Figure 2b). The partially separated pulverized coals were made into polished sections, and the contents of maceral groups were obtained using photometer microscopy. All samples were marked appropriately to distinguish among various samples with different powder sizes and densities. Various subscripts in the nomenclature of samples were as follows: "1" represents 60−80 mesh samples; "2" represents 120−150 mesh samples; "3" represents >200 mesh samples; "L" represents low density samples; "M" represents medium density samples; and "H" represents high density samples.

2.2.2. Methodology of LT-N_2GA and LT-CO_2GA. The LT-N_2GA and LT-CO_2GA experiments were carried out using an ASAP 2020 automated surface analyzer at the experimental temperatures of 77 and 273.15 K, respectively, and following the Chinese Oil and Gas Industry Standard of SY/T 6154-2008. First, about 5 g of different particle size samples was taken out and dried at 378.15 K for 12 h in a vacuum-drying instrument. After degassing, the pulverized coal samples were placed in the analyzer. Based on the different pore size ranges obtained using LT-N_2GA (1.7−300 nm) and LT-CO_2GA (<2 nm) experi-

https://doi.org/10.1021/acsomega.2c07876
ACS Omega 2023, 8, 12079−12097

ments, the analyzer preset different pressure conditions for adsorption/desorption experiments. When calculating the pore volume, surface area, and other parameters, the Barrett−Joyner−Halenda (BJH) method was used in the LT-N_2GA experiments, whereas the density functional theory (DFT) method was used for the LT-CO_2GA experiments.

2.2.3. Methodology of Isothermal Adsorption. Methane adsorption experiments were carried out using an ISO-300 isothermal adsorption instrument at the experimental temperature of 303.15 K (Terra Tek Ltd). The experimental gases included He and CH_4 (purity of 99 vol %). Before experiments, the air tightness and free volume tests of the experimental instrument and the free space volume of the sample cylinder were carried out by using He. The pulverized coal samples (about 30 g, dried at 378.15 K for 12 h)[21] were put in the sample cylinder. After vacuuming, the amount of adsorption was analyzed at different pressure points with the equilibration time of 12 h for each pressure point. The above experiments were repeated for different pulverized coal samples.

In general, to reflect the actual situation of gas adsorption of the samples, the excess adsorption amount is often converted to absolute adsorption amount using eq 1.[53,54]

$$V_e = V_a\left(1 - \frac{\rho_{gas}}{\rho_{ad}}\right) \tag{1}$$

where V_e is the excess adsorption amount, in cm^3/g; V_a is the absolute adsorption amount, in cm^3/g; ρ_{gas} is the gas density, in g/cm^3; and ρ_{ad} is the adsorption phase density, in g/cm^3.

The absolute adsorption amount at each pressure point was fitted to the Langmuir model (eq 2) to obtain the characteristics of the isothermal adsorption curve.

$$V_a = \frac{V_L P}{P + P_L} \tag{2}$$

where V_L is the Langmuir volume, in cm^3/g; P is the gas pressure, in MPa; and P_L is the Langmuir pressure, in MPa.

2.2.4. Methodology of the Adsorption Potential and Adsorption Space. The adsorption potential reflects the work done by the adsorbate while changing from the free phase to the adsorption phase per unit mass.[55,56] When the adsorbate falls into the force field space, it will be affected by the field strength and be adsorbed. Under the action of the adsorption potential field, the adsorption potential can be described using eq 3.[57]

$$\varepsilon = \int_{P_i}^{P_0} \frac{RT}{P} dP = RT \ln \frac{P_0}{P_i} \tag{3}$$

where ε is the adsorption potential, in J/mol; P_0 is the saturated vapor pressure of gas, in MPa; P_i is the equilibrium pressure of ideal gas under a constant temperature, in MPa; R is the molar gas constant, in J/(K·mol); and T is the temperature, in K.

Because the experimental temperature (303.15 K) is higher than the critical temperature of methane (190.6 K), methane cannot be liquefied normally, which makes P_0 meaningless.[58] The Dubinin empirical correlation is often used to replace P_0 with the virtually saturated vapor pressure (P_s) for research, which is given using eq 4.

$$P_s = P_c\left(\frac{T}{T_c}\right)^2 \tag{4}$$

where P_c is the critical pressure such that $P_{c,CH4} = 4.62$ MPa; T_c is the critical temperature such that $T_{c,CH4} = 190.6$ K.

The adsorption space represents the space occupied by the adsorbed gas and can be used as a parameter to characterize the pore structure. It can be calculated using eq 5.[45,58]

$$\omega = V_{ad}\frac{M}{\rho_{ad}} = \frac{V_a M}{1000 V_0 \rho_{ad}} \tag{5}$$

where ω is the adsorption space, in cm^3/g; V_{ad} is the absolute adsorption quantity, in mol/g; M is the molar mass, in g/mol; and V_0 is the molar volume of the gas at standard conditions, in L/mol.

2.2.5. Methodology for Determining Surface Free Energy. Coal has a macromolecular structure, which is mainly composed of aromatic rings that are connected by aliphatic side chains. Ideally, the carbon atoms on the macromolecular skeleton attract each other and reach equilibrium. However, the presence of pores in the macromolecular skeleton can lead to a stress imbalance between the carbon atoms, resulting in a force on the surface of the pores toward the coal body.[59] In this case, according to the theory of surface chemistry, the reduction in surface tension reduction is described using eq 6.

$$-d\sigma = RT\Gamma d(\ln P) \tag{6}$$

where σ is the surface tension, in J/m^2, and Γ is the surface excess, in mol/m^2, which is given by eq 7.

$$\Gamma = \frac{V}{SV_0} = \frac{V_a}{1000 SV_0} \tag{7}$$

where V is the absolute adsorption amount, in L/g; S is the specific surface area, in m^2/g.

Through eqs 6 and 7, the reduction of surface free energy of methane gas can be expressed using eq 8.

$$\Delta\gamma = \frac{V_L RT}{1000 SV_0}\ln\left(1 + \frac{P}{P_L}\right) \tag{8}$$

where $\Delta\gamma$ is the reduction of surface free energy, in J/m^2, which represents the difference in surface free energy before and after the adsorption of gas.

By differentiating the pressure, the rate of change of reduction in surface free energy at different pressure points can be obtained and is expressed using eq 9.

$$\Delta\gamma_P = \frac{V_L RTP_L}{1000 SV_0(P + P_L)} \tag{9}$$

where $\Delta\gamma_P$ is the value of the change in surface free energy at each pressure point, in J/m^2, which represents the difference between the cumulative free energy reductions across two consecutive pressure points.

3. RESULTS AND DISCUSSION

3.1. Separation Characteristics of Different Maceral Groups with Various Ranks. Generally speaking, it has become a consensus that inertinite density > vitrinite density > liptinite density.[60] However, various factors such as coal rank and structural conditions can affect the densities of different maceral groups.[61] Therefore, in this study, to effectively compare the differences of maceral groups, the density of the heavy liquid was appropriately adjusted to meet the separation needs of different coal rank samples. The separation results are presented in Table 2 and Figure 3. It is seen from the results

https://doi.org/10.1021/acsomega.2c07876
ACS Omega 2023, 8, 12079−12097

Table 2. Separation Content of Maceral Groups under Different Particle Sizes and Heavy Liquid Densities

samples	density interval (g/cm^3)	V/H (vol %)	I (vol %)	L (vol %)	samples	density interval (g/cm^3)	V/H (vol %)	I (vol %)	samples	density interval (g/cm^3)	V/H (vol %)	I (vol %)
H_{1L}	<1.34	90.8	8.8	0.4	R_{1L}	<1.25	90.4	9.6	Z_{1L}	<1.4	87.6	12.4
H_{1M}	1.34−1.39	75.5	23.7	0.2	R_{1M}	1.25−1.4	71.6	28.4	Z_{1M}	1.4−1.45	85.1	14.9
H_{1H}	>1.39	72.6	27.2	0.2	R_{1H}	>1.4	56.5	43.5	Z_{1H}	>1.45	67.4	32.6
H_{2L}	<1.34	86.6	12.9	0.5	R_{2L}	<1.25	82.6	17.4	Z_{2L}	<1.4	86.4	13.6
H_{2M}	1.34−1.39	74.3	25.4	0.3	R_{2M}	1.25−1.4	67.4	32.6	Z_{2M}	1.4−1.45	84.2	15.8
H_{2H}	>1.39	56.7	43.1	0.2	R_{2H}	>1.4	45.9	54.1	Z_{2H}	>1.45	61.8	38.2
H_{3L}	<1.34	85.1	14.1	0.8	R_{3L}	<1.25	71.3	28.7	Z_{3L}	<1.4	72.9	27.1
H_{3M}	1.34−1.39	73.4	26.2	0.4	R_{3M}	1.25−1.4	64.8	35.2	Z_{3M}	1.4−1.45	71.6	28.4
H_{3H}	>1.39	63.7	36	0.3	R_{3H}	>1.4	48.7	51.3	Z_{3H}	>1.45	62.5	37.5

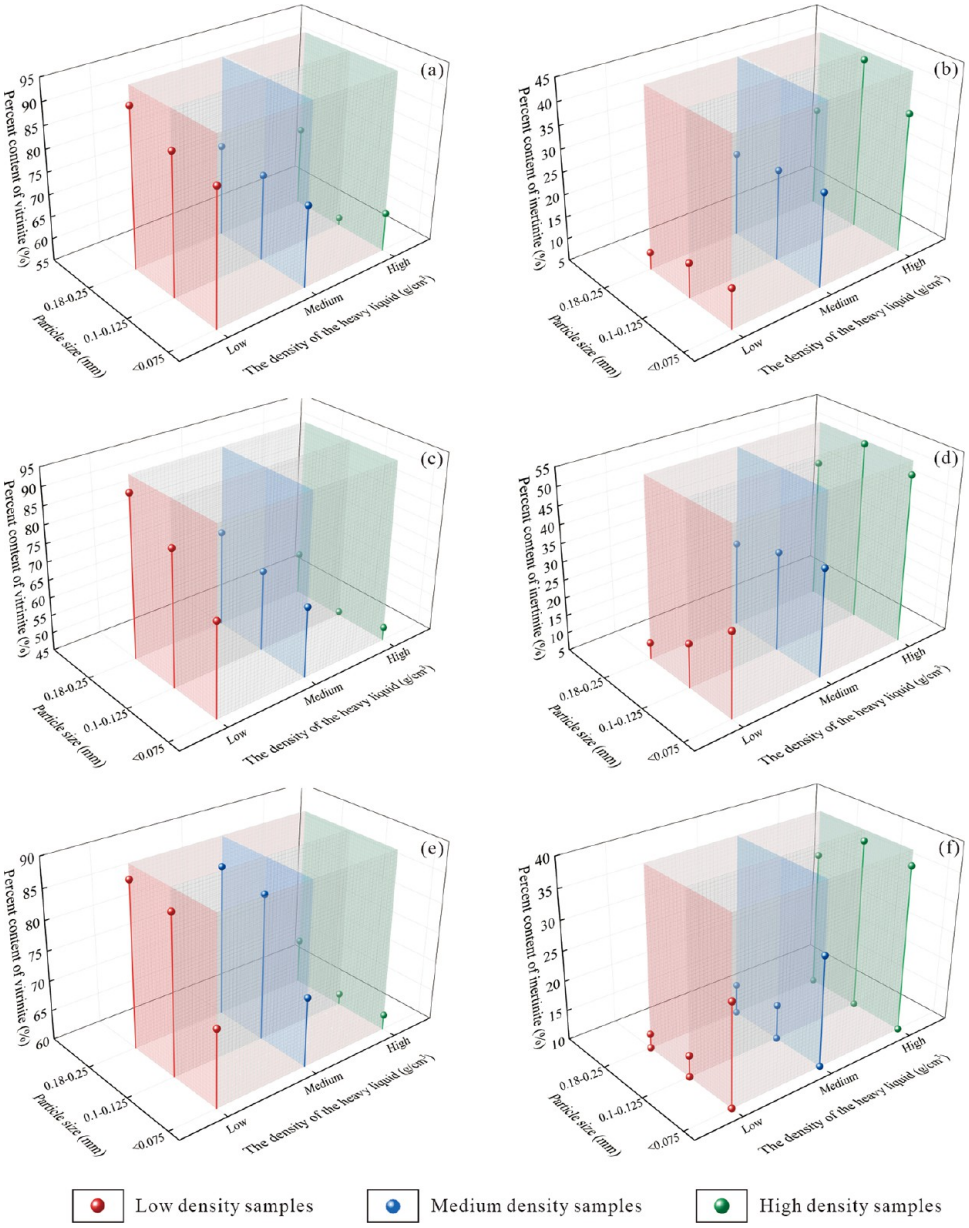

Figure 3. Separation characteristics of maceral groups in samples of various ranks (a, c, e: the distribution characteristics of vitrinite for low-, medium-, and high-rank coal samples; b, d, f: the distribution characteristics of inertinite for low-, medium-, and high-rank coal samples).

presented in Table 2 that the maceral groups of low-, medium-, and high-rank coal samples were mainly vitrinite, and therefore, vitrinite-enriched samples can be obtained (vitrinite content is more than 85 vol %). The effect of particle size on the separation of maceral group separation is shown in Figure 3a−f. For the low and medium densities of heavy liquid samples, the smaller the particle size, the lower the separation content of vitrinite and the higher the separation content of inertinite. For the high density

https://doi.org/10.1021/acsomega.2c07876
ACS Omega 2023, 8, 12079−12097

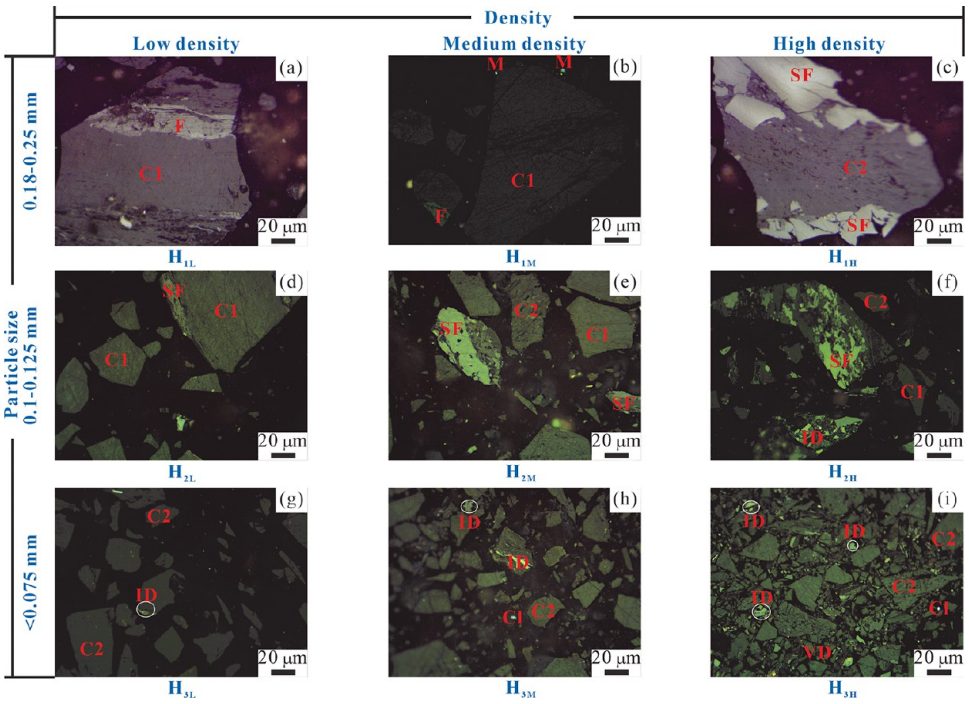

Figure 4. Enrichment characteristics of maceral groups of low-rank coal samples (a–i: H_{1L}–H_{3H}).

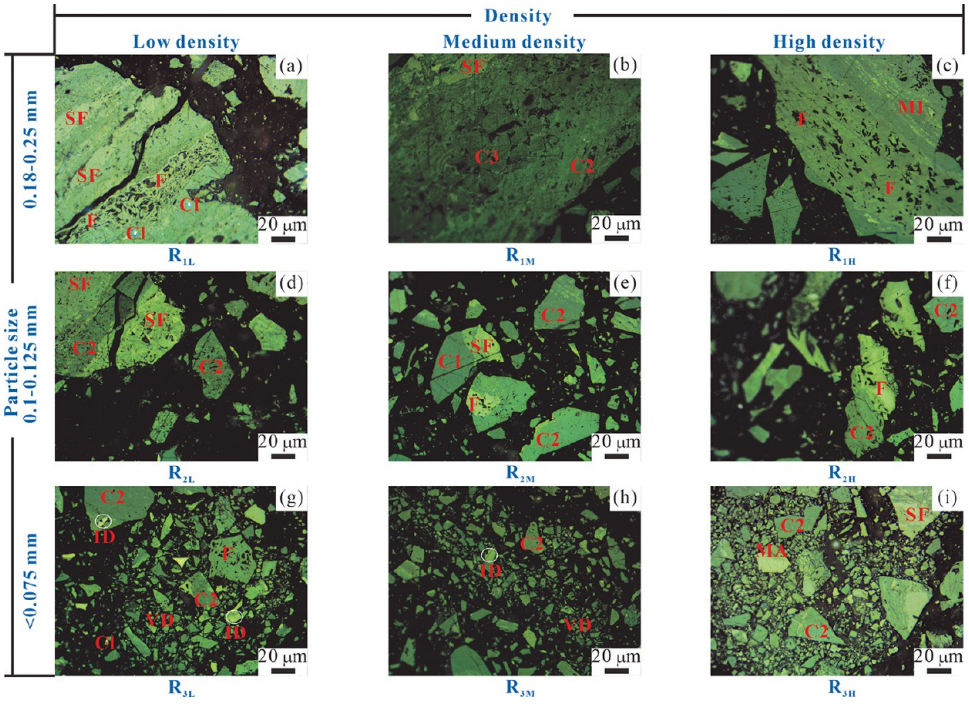

Figure 5. Enrichment characteristics of maceral groups of medium-rank coal samples (a–i: R_{1L}–R_{3H}).

of heavy liquid samples, although the overall variation trend of vitrinite and inertinite remained the same as for the low and medium densities of heavy liquid samples, the optimum separation was achieved for the samples with a particle size of 0.1–0.125 mm. The effect of the density of heavy liquid on the separation of maceral groups is also shown in Figure 3a–f. For the samples with different particle sizes, the higher the density of the heavy liquid, the lower the separation content of the vitrinite, and the higher the separation content of inertinite.

The maceral groups of all the samples under reflected polarized light (oil immersed) are shown in Figures 4–6. From the point of view of the morphology of particles, with the decrease of particle size, the degree of fragmentation of maceral groups improved, but it will be relatively more enriched. As the density of heavy liquid increased, the content of inertinite increased. The maceral groups were mainly composed of vitrinite, including telocollinite (C1), desmocollinite (C2), corpogelinite (C3), and vitrodetrinite (VD), followed by inertinite that included fusinite (F), semifusinite (SF), macrinite

https://doi.org/10.1021/acsomega.2c07876
ACS Omega 2023, 8, 12079–12097

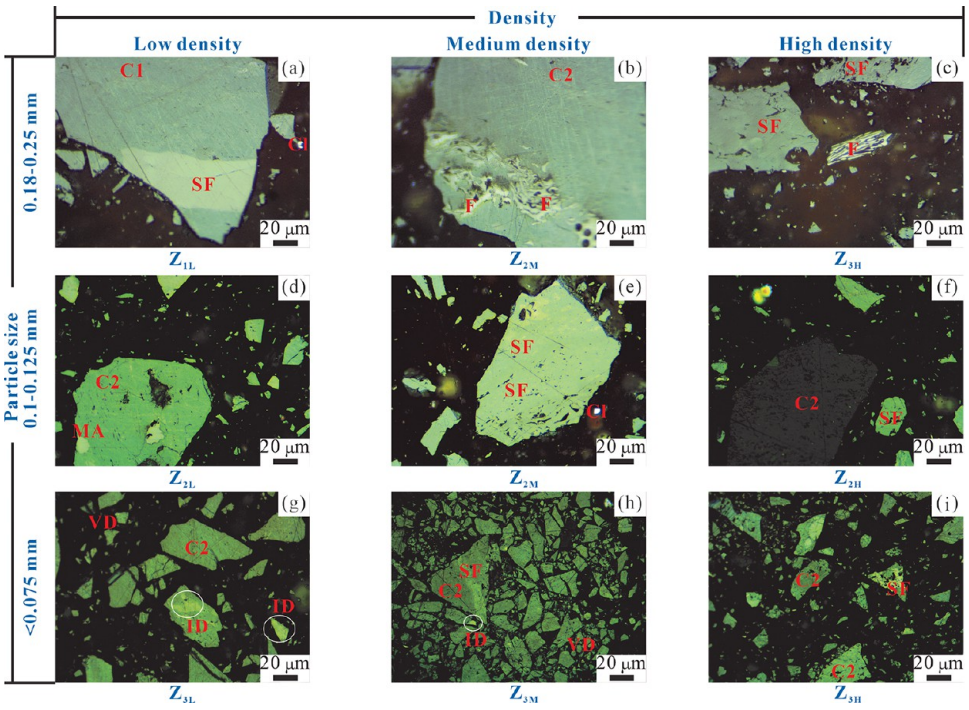

Figure 6. Enrichment characteristics of maceral groups of high-rank coal samples (a–i: Z_{1L}–Z_{3H}).

(MA), micrinite (MI), and inertodetrinite (ID), with only a few minerals (M).

3.2. Pore Characteristics of Different Maceral Groups with Various Ranks Using LT-N_2GA. *3.2.1. Evolutionary Characteristics of LT-N_2GA Isotherms.* Figure 7 shows the detailed characteristics of isothermal adsorption curves. First, it is seen from the adsorption branches that, when relative pressure (P/P_0) was less than 0.9, the amount of N_2 adsorbed increased slowly, suggesting a gradual conversion from monolayer adsorption to multilayer adsorption. When P/P_0 was greater than 0.9, the amount of N_2 adsorbed increased rapidly, indicating that capillary condensation occurred.[62] Therefore, the LT-N_2GA isothermal adsorption curves belonged to type IV isotherms.[63,64] Second, the desorption and adsorption branches of some samples did not overlap at high pressure, indicating that hysteresis loops existed. According to the delineation by IUPAC, the hysteresis loops can be classified into three types.[65] Type I is characterized by almost overlapping adsorption and desorption branches, whereas the hysteresis loops are weak or non-existent, such as R_{2L}, which indicates that it is dominated by semi-closed pores with poor connectivity in the samples, such as wedge-shaped pores and cylinder cavity closed at one end. Type II has significant hysteresis loops at relatively high pressure. However, the adsorption and desorption branches overlap at relatively low pressure, such as Z_{2H}, which indicates that it is dominated by the large open pores with better connectivity, such as cylindrical pores and parallel plane pores, and small semi-closed pores in the samples. Type III is similar to type II, except that the desorption branch appears to have a sudden drop at the P/P_0 of about 0.45. Moreover, the hysteresis loop is more significant than type II, such as H_{1H}, which shows that the pore type is dominated by narrow neck and wide body pores, such as ink-bottle-shaped pores.

Within the same particle size interval, the type of the hysteresis loop of the samples with various ranks changed with the increase in vitrinite content as follows: low-rank coal samples changed from type III to type II (Figure 7a–c); medium-rank coal samples remained type I (Figure 7d–f); and high-rank coal samples changed from type III or type II to type I (Figure 7g–i). The results show that the samples rich in vitrinite generally had more semi-closed pores, while samples rich in inertinite generally had more open pores. In addition, it is seen in Figure 7a–c that the vitrinite content of H_{2M} was 74.3 vol %, which differed from those of H_{1M} and H_{3M} by 1.2 and 0.9 vol %, respectively. Therefore, the variation characteristics of the hysteresis loop from H_{1M} to H_{3M} can be approximately regarded as the influence of particle size and the decreasing hysteresis loop with H_{1M}, H_{2M}, and H_{3M} suggests that the particle size is also able to influence the morphological characteristics of the pores to some extent.

3.2.2. Characteristics of the LT-N_2GA Pore Structure. Results on the pore structure of various samples are presented in Table 3 and Figures 8 and 9. In this study, the classification of pore structure is based on Hodot pore classification. Pores are divided into ultra-micropores (<2 nm), micropores (2–10 nm), transition pores (10–100 nm), mesopores (100–1000 nm), and macropores (1000–20,000 nm). It is clear that due to the orientation effect of nitrogen molecules and the fact that the cross-sectional area of nitrogen molecules is smaller than the recognized area (0.162 nm^2), inaccurate results for micropores were obtained.[66,67] Thommes et al.[65] and Bertier et al.[68] conducted related research and found that the BJH model underestimated the pores (<10 nm), while the error can be as high as 20–30 vol % as compared to the actual values. Therefore, when calculating the BJH pore volume and surface area, the micropores are not considered.

The pore volume and surface area of samples with the same particle size interval increased with the increase in inertinite content (Figures 8 and 9), indicating that inertinite can provide more pore volume and surface area than vitrinite in transition pores and mesopores, which is consistent with the results of Louw et al.[69] Vitrinite and inertinite are mainly formed through

https://doi.org/10.1021/acsomega.2c07876
ACS Omega 2023, 8, 12079–12097

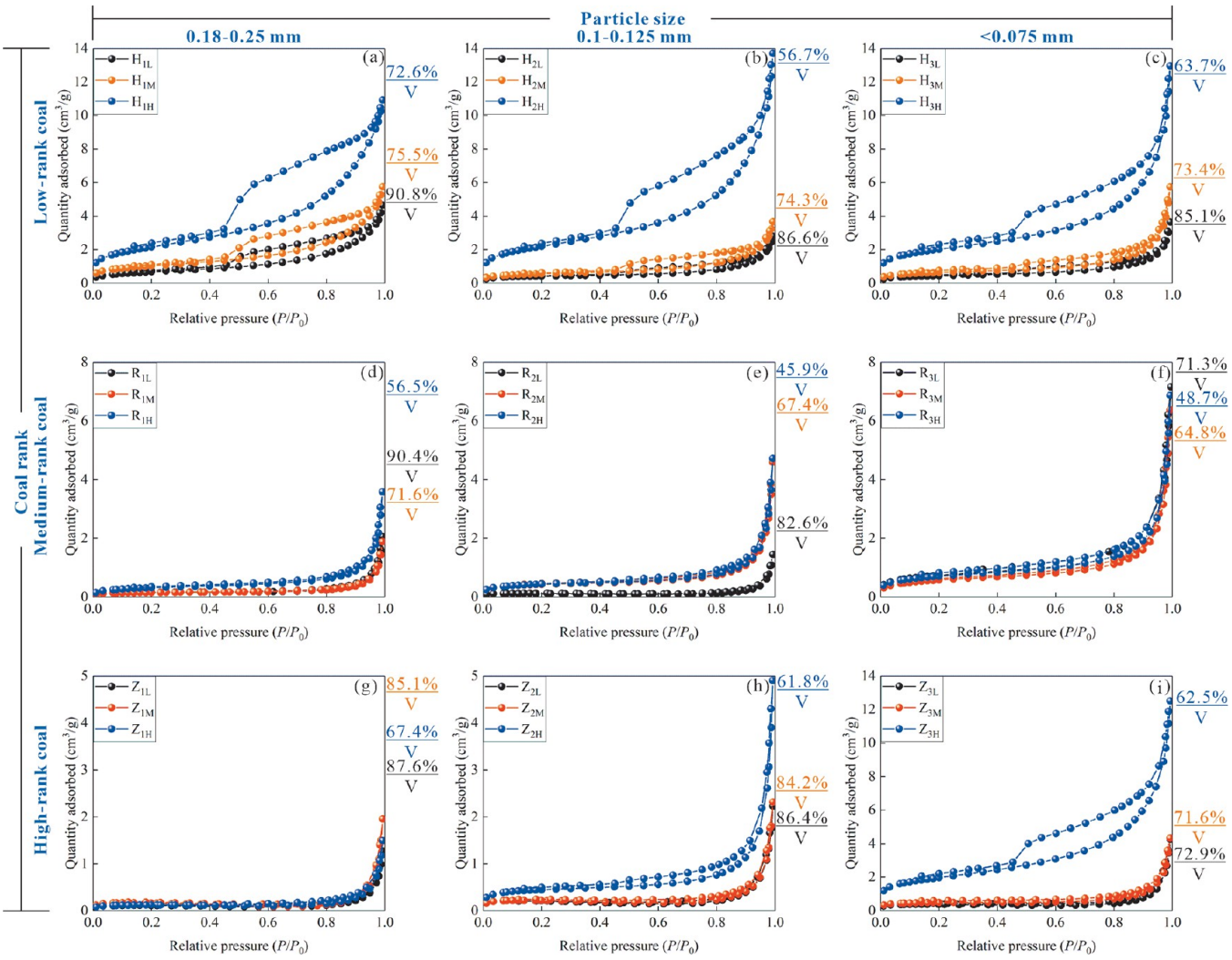

Figure 7. N_2 adsorption and desorption isotherms (a−c, d−f, and g−i: low-, medium-, and high-rank coal samples at particle sizes of 0.18−0.25, 0.1−0.125, and <0.0075 mm, respectively).

Table 3. Characteristic Parameters of Pore Structure Derived from LT-N_2GA[a]

		pore volume ($\times 10^{-3}$ cm^3/g)					pore volume ($\times 10^{-3}$ cm^3/g)					pore volume ($\times 10^{-3}$ cm^3/g)		
SN	S_{BJH} (m^2/g)	V_{BJH}	V_1	V_2	SN	S_{BJH} (m^2/g)	V_{BJH}	V_1	V_2	SN	S_{BJH} (m^2/g)	V_{BJH}	V_1	V_2
H_{1L}	0.69	5.17	3.73	1.44	R_{1L}	0.23	2.99	1.55	1.44	Z_{1L}	0.14	1.82	0.97	0.85
H_{1M}	0.84	5.96	4.46	1.50	R_{1M}	0.21	2.71	1.39	1.32	Z_{1M}	0.24	3	1.62	1.38
H_{1H}	1.68	10.54	8.41	2.13	R_{1H}	0.42	5	2.71	2.29	Z_{1H}	0.18	2.16	1.18	0.98
H_{2L}	0.39	3.45	2.34	1.11	R_{2L}	0.15	2.08	1.01	1.07	Z_{2L}	0.28	3.39	1.92	1.47
H_{2M}	0.5	4.28	2.87	1.41	R_{2M}	0.52	6.47	3.35	3.12	Z_{2M}	0.28	3.46	1.89	1.57
H_{2H}	2	15.01	10.85	4.16	R_{2H}	0.54	6.62	3.54	3.08	Z_{2H}	0.57	6.95	3.96	2.99
H_{3L}	0.44	4.6	2.76	1.84	R_{3L}	0.79	7.66	5.74	1.92	Z_{3L}	0.51	6.15	3.62	2.53
H_{3M}	0.75	7.5	4.57	2.93	R_{3M}	0.74	8.85	4.68	4.17	Z_{3M}	0.53	6.02	3.44	2.58
H_{3H}	1.75	14.89	9.99	4.90	R_{3H}	0.8	9.29	5.47	3.82	Z_{3H}	1.72	14.25	9.66	4.59

[a]SN: sample number, dimensionless; S_{BJH}: BJH surface area (>10 nm), m^2/g; V_{BJH}: BJH pore volume (>10 nm), 10^{-3} cm^3/g; V_1: pore volume of transition (10−100 nm), 10^{-3} cm^3/g; V_2: pore volume of mesopores (>100 nm), 10^{-3} cm^3/g; S_1: surface area of transition pores (10−100 nm), m^2/g; S_2: surface area of mesopores (>100 nm), m^2/g.

biochemical processes after the burial of higher plants. Due to the presence of unstable compounds such as proteins, the cavity is constantly broken down by the action of bacteria and enzymes. At the same time, the cell wall becomes more stable than the cell cavity. Thus, it can be preserved under different coal-forming conditions. Plant tissues need to undergo humification to form vitrinite eventually.[70] Therefore, in the early stages of coalification, inertinite itself has a large number of plant tissue pores while vitrinite is not developed. The higher the content of inertinite in low-rank coal samples, the larger the volume and surface area. With the deepening of coalification, the generation of hydrocarbon of vitrinite begins to strengthen,

https://doi.org/10.1021/acsomega.2c07876
ACS Omega 2023, 8, 12079−12097

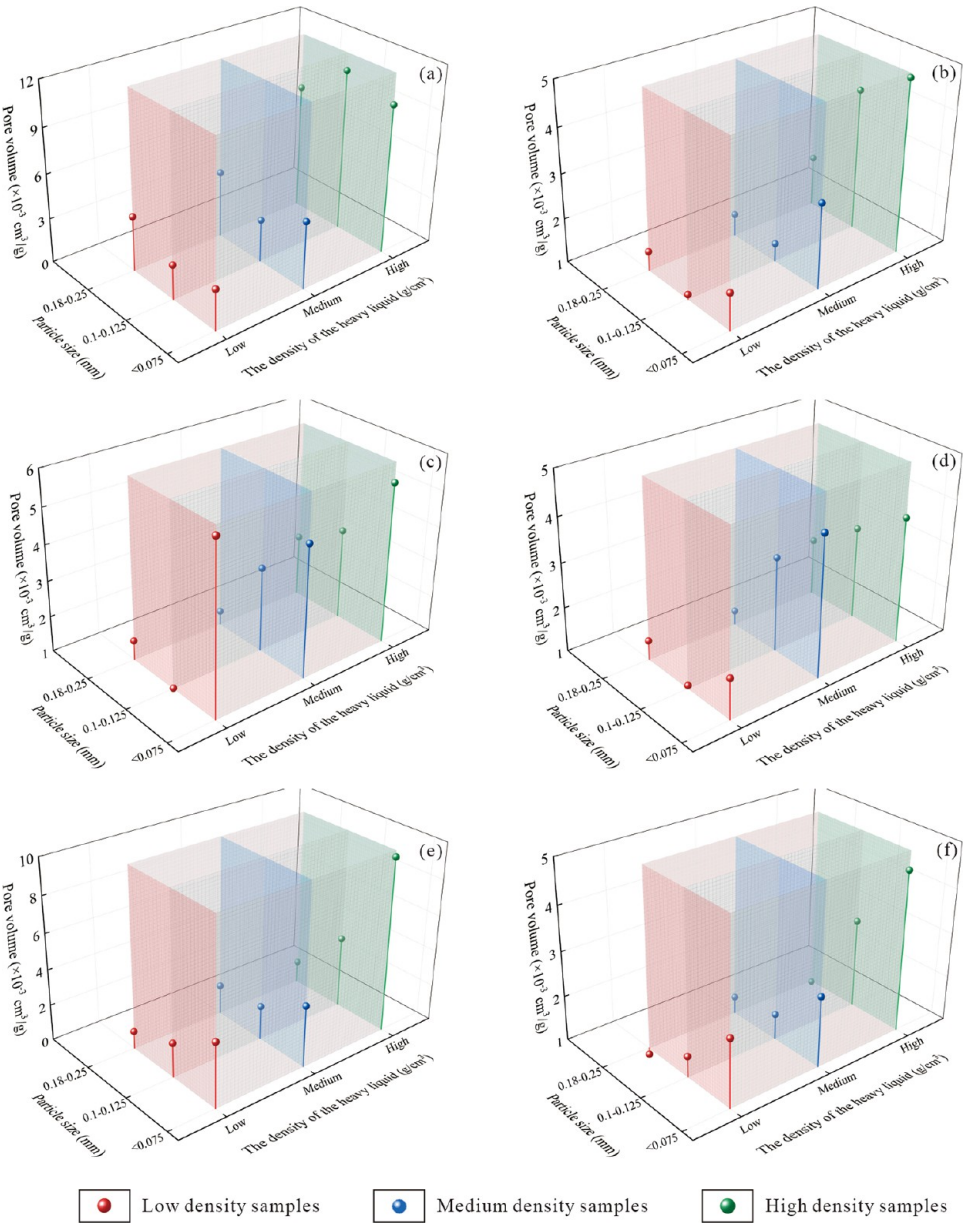

Figure 8. Distribution of pore volume under different particle sizes and heavy liquid densities from LT-N_2GA (a, c, e: the distribution characteristics of volume of transition pores for low-, medium-, and high-rank coal samples; b, d, f: the distribution characteristics of volume of mesopores for low-, medium-, and high-rank coal samples).

resulting in the appearance of gas pores and a large number of micropores. Therefore, due to the enrichment of gas pores in the medium- and high-rank coal samples,[71] certain anomalies such as R_{1L} and Z_{1M} appear. Because of the limitations of the experimental methods in this study, the variation characteristics of micropores are not discussed.

In addition, some unique phenomena can also be observed. The first special phenomenon is exemplified by the samples H_{1M} and H_{1H}, which have similar contents of vitrinite and inertinite. However, the differences in pore volume and surface area were nearly twice as large. The main reason for this phenomenon is that the inertinite is mainly dominated by fusinite, which develops a unique stripped fiber structure with different evolutionary effects, resulting in tissue pores showing remarkable differences in the pore structure.[61,72] For the second extraordinary phenomenon, the samples of R_{3L} and R_{3M} are considered as an example. The total pore volume increased, while the total surface area decreased. This phenomenon is mainly because the increase in mesopores and macropores (>100 nm) makes a very limited contribution to the surface area, due to which the decrease in transition pores leads to a decrease in the surface area.

The results obviously showed that the particle size had little effect on pore volume and surface area (Figures 8 and 9). The vitrinite content was 90.8, 86.6, and 85.1 vol % for H_{1L}, H_{2L}, and H_{3L}, respectively. The pore volume and surface area values first decreased and then increased with the decrease in particle size. The same variation pattern was observed for the low-rank coal samples (H_{1M}, H_{2M}, and H_{3M}) and medium-rank coal samples (R_{1L}, R_{2L}, and R_{3L}). These results suggested that inertinite did not provide more pore volume and surface area than vitrinite. However, the analysis of low-rank samples (H_{1H}, H_{2H}, and H_{3H}), medium-rank coal samples (R_{1M}, R_{2M}, and R_{3M}, and R_{1H}, R_{2H}, and R_{3H}), and high-rank coal samples supported the inference

https://doi.org/10.1021/acsomega.2c07876
ACS Omega 2023, 8, 12079−12097

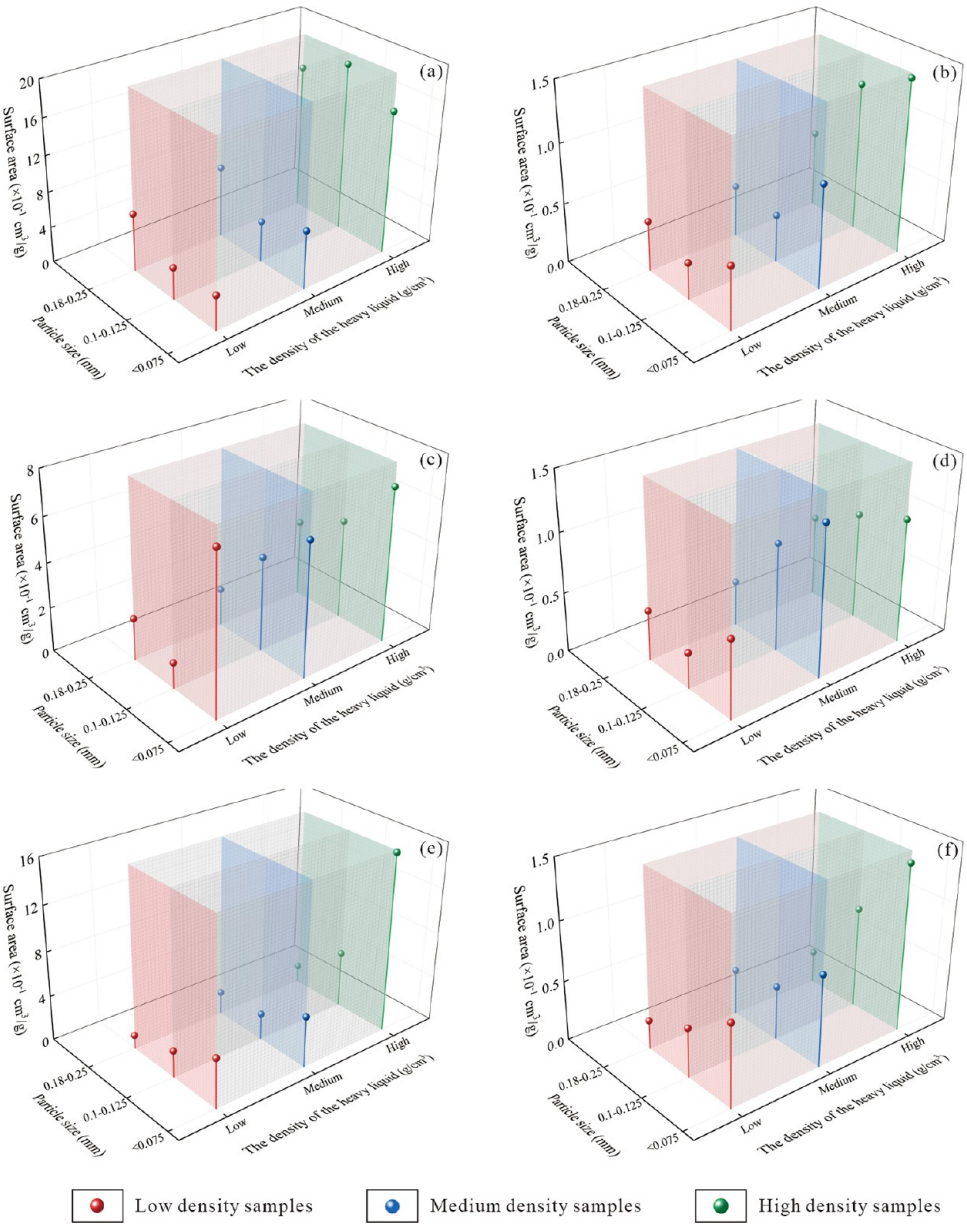

Figure 9. Distribution of surface area under different particle sizes and heavy liquid densities from LT-N_2GA (a, c, e: the distribution characteristics of surface area of transition pores for low-, medium-, and high-rank coal samples; b, d, f: the distribution characteristics of surface area of mesopores for low-, medium-, and high-rank coal samples).

that inertinite can provide more pore volume and surface area. The results further showed that the particle size had little influence on the change of pore structure, and the effect of particle size on pore structure decreased with the increase of coal rank. However, Mastalerz et al.[73] and Zhang et al.[19] reported that when the particle size was less than 0.25 mm, its influence on the change of total pore volume and surface area was small and negligible. Zhang et al.[19] and Wang et al.[74] found that when the particle size was less than 0.25 mm, the change in the volume of macropores was tiny, while the increment was about 0.00003−0.0001 cm^3/g. In this paper, the increments of macropores with different particle sizes significantly exceeded this value. Therefore, the changes in pore volume and surface area of the samples are mainly caused by vitrinite and inertinite. The particle size had an impact on the change of pore volume and surface area. Moreover, compared with the influence of maceral groups, the effect of particle size on the variation in pore volume and surface area was very limited.

The effect of particle size on the pore structure is seen in Figure 10. This can be due to the following reasons: (1) From the perspective of the pores, with the decrease of particle size, some closed pores may have opened, contributing to detectable pore volume and surface area (Figure 10a,b) or leading to the destruction of some pores, thus reducing the contribution of these pores to pore volume and surface area (Figure 10b,c). (2) From the point of view of inorganic minerals, with the decrease in particle size, the minerals may fall off from the matrix or pores during the crushing process, forming some mineral pores.[62,75] (3) From the perspective of the brittleness of maceral groups, vitrinite is more brittle, while inertinite is harder. Therefore, it is more easily controlled by particle size for samples rich in vitrinite, while it is relatively weakly influenced by particle size of samples rich in inertinite.[76] (4) From the point of view of

https://doi.org/10.1021/acsomega.2c07876
ACS Omega 2023, 8, 12079−12097

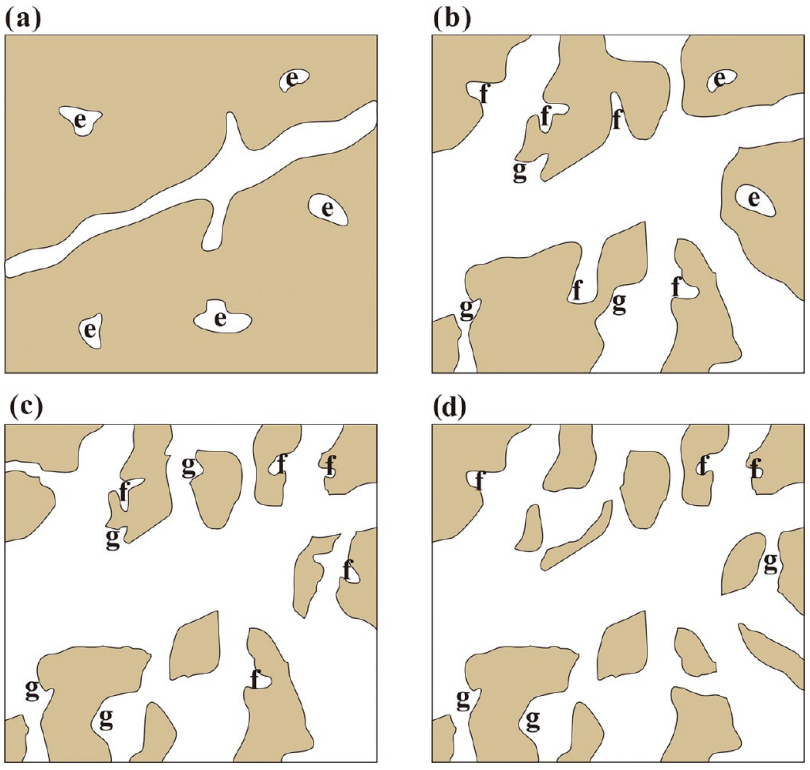

Figure 10. Schematic of the influence of particle sizes on pore structure (a−c: effect of particle size on pores; d: effect of external forces on pores; e: closed pores; f: micropores filling; g: external surface).

external interference, the samples may generate artificial pores and fissures during the crushing process.[77,78] Due to the inhomogeneous and fragile nature of coal, with the decrease in particle size, the samples will be subjected to specific external forces, which will affect the contribution of these pores to the pore volume and surface area (Figure 10d).

3.2.3. Pore Size Distribution Characteristics. The PSD of the samples is shown in Figure 11. With the increase in pore diameter, the incremental pore volume of different curves first increased, and then decreased, followed by another increase. The incremental pore volume of all samples reached the maximum value within the pore diameter range of 40−50 nm and the minimum value for the pore diameter of around 80 nm. It is noteworthy that the maximum incremental pore volume increased with the increase in inertinite content and the minimum incremental pore volume increased with the increase in vitrinite content. This phenomenon reflects that in the transition pores, the pores of 40−50 nm are more developed in inertinite while the pores around 80 nm are more developed in vitrinite.

3.3. Pore Characteristics of Different Maceral Groups with Various Ranks Using LT-CO_2GA. *3.3.1. Evolutionary Characteristics of LT-CO_2GA Isotherms.* Because the kinetic diameter of carbon dioxide (0.33 nm) is smaller than that of nitrogen (0.364 nm) and the presence of the difference in thermal energy is caused by the experimental temperatures (77 and 273.15 K), LT-CO_2GA can measure smaller pores than LT-N_2GA adsorption experiments. Moreover, LT-CO_2GA exhibited a typical characteristic of the type I isothermal adsorption curve, with a rapid increase in adsorption at low pressure, which is similar to the results obtained in previous work (Figure 12).[79]

For all the samples, the amount of adsorbed CO_2 increased with the increase of vitrinite content. The adsorbed amount of CO_2 was found in the following descending order for various samples: $H_{1M} > H_{1L} > H1_H > H_{2H}$ in low-rank coal samples; $R_{2L} > R_{3H} > R_{1H} > R_{2H}$ in medium-rank coal samples; $Z_{1L} > Z_{1M} > Z_{1H} > Z_{3H}$ in high-rank coal samples.

3.3.2. Characteristics of the LT-CO_2GA Pore Structure. The results for the pore structure for various samples are presented in Table 4 and Figure 13. For the same particle size, the pore volume and surface area of samples with various ranks decreased with the increase of inertinite content (Figure 13a−c), indicating that vitrinite can provide more pore volume and surface area of ultra-micropores than inertinite. Interestingly, the samples H_{1M} and H_{1H} that have similar vitrinite contents (75.5 and 72.6 vol %) exhibited significantly different pore volumes and surface areas from each other. It is consistent with the variation in transition pores, mesopores, and macropores in H_{1M} and H_{1H}, reflecting the difference of tissue pores in pore structure. However, the influence of sub-maceral groups cannot be ignored. In addition, in terms of the decrease in pore volume and surface area, the decrease in surface area was always smaller than the decrease in pore volume. It can be concluded that the ultra-micropores in inertinite are larger than those in vitrinite.

From the point of view of particle size, for the medium-rank coal samples R_{2H} and R_{3H} (V: 45.9 and 48.7 vol %), the volume and surface area increased with the decrease of particle size, whereas for the high-rank coal samples Z_{1H} and Z_{3H} (V: 67.4 and 62.5 vol %), the volume and surface area decreased with the decrease of particle size. The effect of particle size was not discussed for the low-rank coal samples H_{1H} and H_{2H} due to the difference in the contents of vitrinite of H_{1H} and H_{2H} (72.6 and 56.7 vol %). The variation of R_{2H}, R_{3H}, Z_{1H}, and Z_{3H} shows no correlation between the particle size and the ultra-micropore

https://doi.org/10.1021/acsomega.2c07876
ACS Omega 2023, 8, 12079−12097

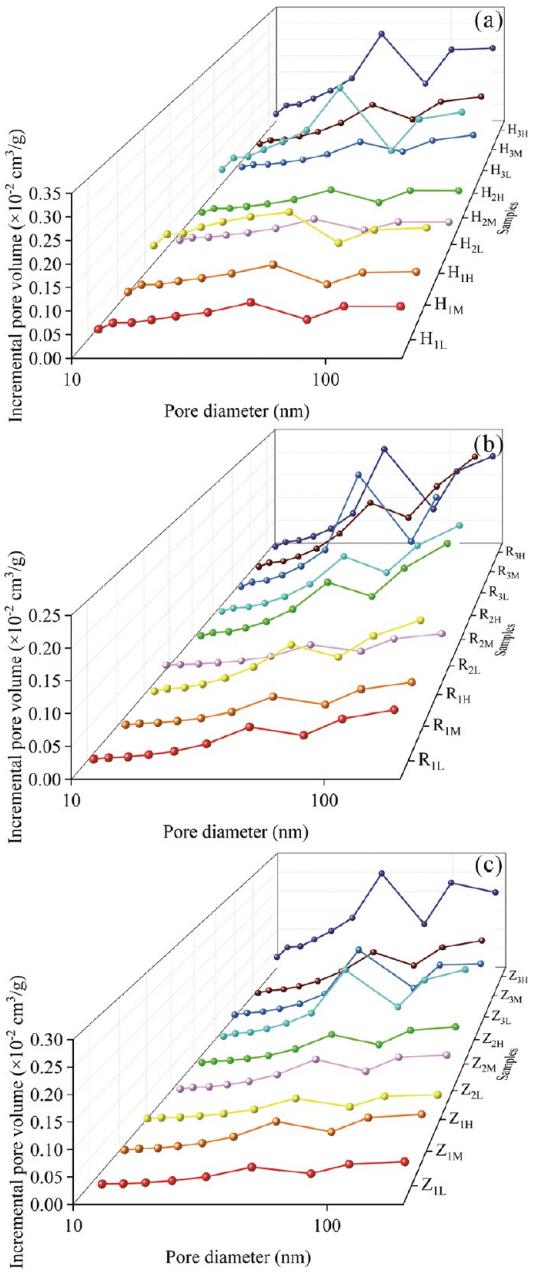

Figure 11. PSD characteristics based on the BJH method (a−c: low-, medium-, and high-rank coal samples with different particle sizes and heavy liquid densities, respectively).

structure. Moreover, the changes in the structure of ultra-micropores are consistent with the conclusion that vitrinite can provide more ultra-micropores. In addition, based upon LT-CO_2GA analysis of coal with different particle sizes, Hou et al.[62] and Mastalerz et al.[73] showed that when the particle size was less than 0.38 mm, the particle size did not affect the characteristics of micropores. Therefore, particle size has essentially no effect on the pore structure of ultra-micropores, whereas the changes in pore volume and surface area are mainly caused by vitrinite and inertinite.

3.3.3. Characteristics of the Size Distribution of Ultra-Micropores. Figure 14 shows the pore size distribution of ultra-micropores (UPSD) for various samples. The UPSD of all samples shows multi-peak characteristics. With the increase of vitrinite content, the number of peaks within the pore diameter

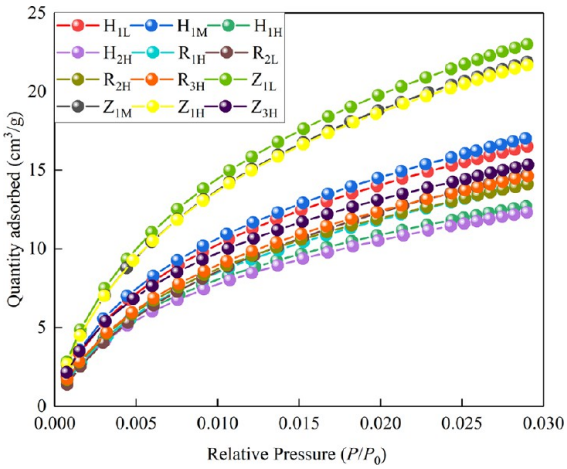

Figure 12. CO_2 adsorption isotherms for different samples.

range of 0.4−0.65 nm of low-, medium-, and high-rank coal samples changed from 5 to 4, which showed that the number of peaks decreased, although the values of peaks increased. With the increase in inertinite content, the number of peaks in the pore diameter (>0.7 nm) of low-, medium-, and high-rank coal samples was diverse, and the values of peaks showed an overall increasing trend. This phenomenon reflects that the ultra-micropores (0.4−0.65 nm) are more developed in vitrinite, while ultra-micropores (>0.7 nm) are more developed in inertinite.

3.4. Methane Adsorption Characteristics of Different Maceral Groups with Various Ranks. Based upon the discussion presented in Sections 3.2 and 3.3, it is inferred that the influence of particle size on the structure of pores is limited relative to the influence of maceral groups. In addition, the gas adsorption sites are mainly provided by the surface area of ultra-micropores in the isothermal adsorption experiments. Therefore, in this study, the relative influence of particle sizes is not considered when discussing the variation in the adsorbed amount of CH_4, starting with the characteristics of maceral groups and pore structure.

Figure 15 shows the characteristics of isothermal adsorption curves of CH_4 for samples with various ranks, whereas the fitting results are presented in Table 5. In the low-rank coal samples, with the increase of inertinite content, the amount of adsorbed CH_4 gradually increased (Figure 15a). In the medium- and high-rank coal samples, the amount of adsorbed CH_4 increased gradually with the increase of vitrinite content (Figure 15b,c). It is seen in Figure 15d that the fitting relationship between the Langmuir volume and the vitrinite content is good, indicating that the amount of adsorbed CH_4 is controlled by inertinite in low-rank coal samples and vitrinite in medium- and high-rank coal samples. In addition, it is seen in Figure 15e that the amount of adsorbed CH_4 shows a U-shaped variation from low-rank to high-rank coal.

The amount of adsorbed methane is mainly controlled by pore and molecular structures of colas. From the point of view of pore structure, it is generally accepted that ultra-micropores play an essential role in gas adsorption. The more the ultra-micropores, the larger the surface area, and the more the adsorption sites (Figure 15f).[46] The adsorption results for methane from the samples show that the adsorption capacity decreased with the increase of vitrinite content in the low-rank coal samples. However, in this study, the ultra-micropores are

https://doi.org/10.1021/acsomega.2c07876
ACS Omega 2023, 8, 12079−12097

Table 4. Characteristic Parameters of Pore Structure Derived from LT-CO_2GA[a]

samples	V_{DFT} ($\times 10^{-2}$ cm^3/g)	S_{DFT} (m^2/g)	samples	V_{DFT} ($\times 10^{-2}$ cm^3/g)	S_{DFT} (m^2/g)	samples	V_{DFT} ($\times 10^{-2}$ cm^3/g)	S_{DFT} (m^2/g)
H_{1L}	2.45	67.93	R_{1H}	1.94	50.67	Z_{1L}	3.65	106.87
H_{1M}	2.53	70.87	R_{2L}	2.14	59.87	Z_{1M}	3.49	103.23
H_{1H}	1.91	55.62	R_{2H}	2.04	59.01	Z_{1H}	3.44	94.77
H_{2H}	1.87	55.70	R_{3H}	2.15	61.73	Z_{3H}	2.27	63.35

[a]S_{DFT}: ultra-micropore total special surface area (0.48−1.05 nm), m^2/g; V_{DFT}: ultra-micropore total pore volume (0.48−1.05 nm), cm^3/g.

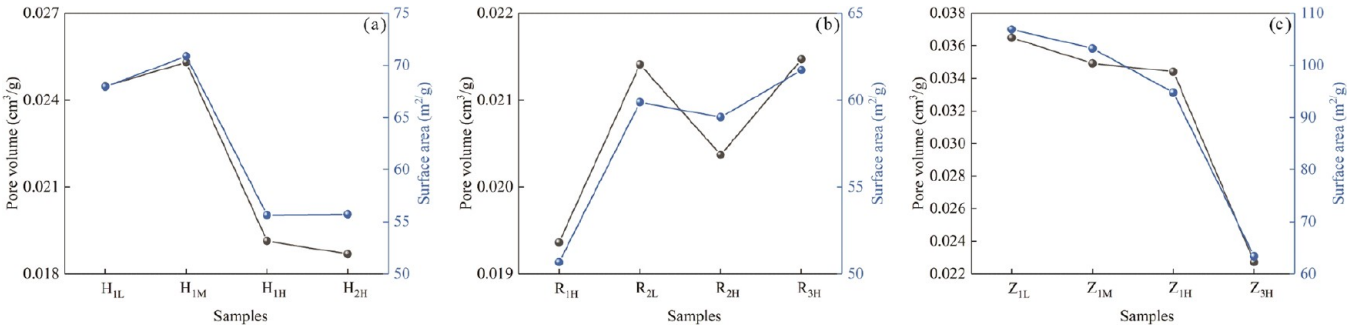

Figure 13. Distributions of pore volume and surface area under different particle sizes and heavy liquid densities derived from LT-CO_2GA (a−c: low-, medium-, and high-rank coal samples, respectively).

mainly provided by vitrinite, which contradicts the view that the more there are ultra-micropores, the greater the adsorption capacity. The reason for this phenomenon can be found in the molecular structure. It should be noted that there are two main differences between the vitrinite and the inertinite.[80−82] First, the aliphatic side chain of inertinite is not affected by the degree of metamorphism. However, for vitrinite, the length of the aliphatic side chain decreases with the deepening of metamorphism. Second, the degree of polycondensation of the aromatic ring of inertinite is basically not affected by the degree of metamorphism, while that of vitrinite increases with the degree of metamorphism.

From the point of view of the molecular structure, the gas adsorption capacity shows that the aromatic ring is stronger than the aliphatic side chain and oxygen functional groups. Although the samples were rich in vitrinite for the low-rank coal samples, the degree of polycondensation of the aromatic ring of vitrinite was low and the aliphatic side chain was relatively long, due to which it had a weak impact on gas adsorption (H_{1L} and H_{1M}). Meanwhile, the degree of polycondensation of the aromatic ring of inertinite is higher than vitrinite,[83] and therefore, it has a stronger controlling effect on gas adsorption (H_{2H}). In addition, in the low-rank coal samples, the relative abundance of aromatic functional groups in vitrinite was less than that in inertinite.[82] Therefore, the adsorption capacity of functional groups in inertinite was stronger than that in vitrinite. Moreover, the higher the content of inertinite, the stronger the amount of adsorbed CH_4. For medium- and high-rank coal samples, the degree of polycondensation of aromatic rings and the abundance of functional groups of vitrinite will increase with the deepening of metamorphism and eventually exceed those of inertinite,[84] thus leading to vitrinite having a stronger effect on gas adsorption than inertinite. As a result, the higher the vitrinite content, the stronger the adsorption capacity. Finally, under the dual action of molecular and pore structure, it is inferred that the amount of adsorbed CH_4 for low-rank coal samples lies between the corresponding amounts for the medium-rank and high-rank coal samples.

3.5. Adsorption Thermodynamics of Different Maceral Groups with Various Ranks. *3.5.1. Characteristics of the Adsorption Potential and Adsorption Space.* The adsorption potential and adsorption space can be calculated using eqs 4 and 6 (Figure 16). For a sample, the adsorption potential and the adsorption space are independent of each other and are not affected by temperature and pressure.[44] The relationship can be given using eq 10.

$$\varepsilon = a\ln(\omega) + b \tag{10}$$

where a and b are the fitting parameters, dimensionless.

It is seen in Figure 16 that the larger the adsorption space of the samples, the smaller the adsorption potential. For the same adsorption potential, the adsorption space of the samples is found to be lying in the following descending order: $\omega_{H2H} > \omega_{H1M} > \omega_{H1L}$, $\omega_{R2L} > \omega_{R2M} > \omega_{R1H}$, and $\omega_{Z1L} > \omega_{Z1M} > \omega_{Z2M} > \omega_{Z2H}$. The larger the adsorption space, the higher the amount of adsorbed gas. Similarly, for the same adsorption space, the adsorption potential of the samples is found to be lying in the following descending order: $\varepsilon_{H2H} > \varepsilon_{H1M} > \varepsilon_{H1L}$, $\varepsilon_{R2L} > \varepsilon_{R2M} > \varepsilon_{R1H}$, and $\varepsilon_{Z1L} > \varepsilon_{Z1M} > \varepsilon_{Z2M} > \varepsilon_{Z2H}$. The larger the adsorption potential, the lower the equilibrium pressure, and the greater the amount of adsorbed CH_4. These results show that the adsorption potential and adsorption space of coal samples with high inertinite content are larger than those with high vitrinite content under the same conditions in low-rank coal samples. Meanwhile, the adsorption potential and adsorption space of coal samples with high vitrinite content are larger than those with high inertinite content under the same conditions in medium−high-rank coal samples. Therefore, the changes of adsorption potential and adsorption space of the samples also confirmed the results of the methane isothermal adsorption experiments.

In addition, based upon the volume filling theory of methane, it is well-known that the adsorbed gas is preferentially filled in the micropores. The relationship between the adsorption potential and the adsorption space shows that the adsorption potential of the samples gradually decreases with the mesopores and macropores being filled (the adsorption space becomes

https://doi.org/10.1021/acsomega.2c07876
ACS Omega 2023, 8, 12079−12097

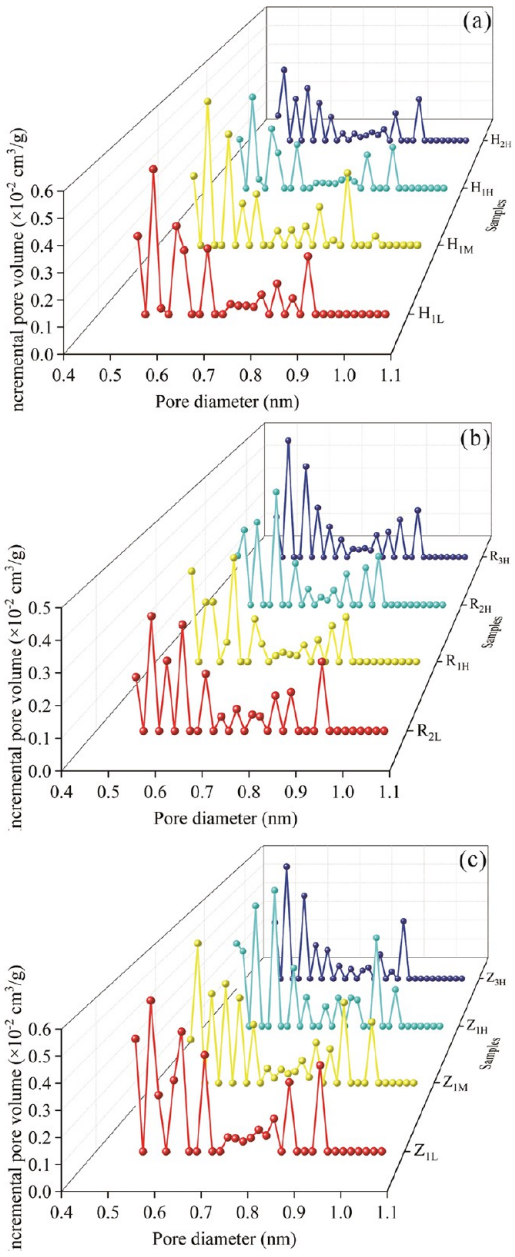

Figure 14. UPSD characteristics based on the DFT method (a, b, and c—low-, medium-, and high-rank coal samples with different particle sizes and heavy liquid densities, respectively).

larger). Due to this reason, the micropores have an extremely high adsorption potential. Previous studies have shown that when the pore size is less than 3.8 nm,[85,86] the adsorption potential would be superimposed (which may be caused by the van der Waals' forces), increasing the adsorption capacity of micropores or ultra-micropores. Therefore, it can be concluded that the more there are ultra-micropores in the samples, the greater the adsorption capacity for the gas. According to the distribution characteristics of ultra-micropores of different coal rank samples (as shown in Figure 13), the medium- and high-rank coal samples conform to the positive effect of methane adsorption by the ultra-micropores, while the low-rank coal samples exhibited the opposite trend. However, with regard to the macromolecular structure, the adsorption energy is similar to the adsorption potential. The aromatic ring contributes the most to the adsorption energy, followed by the oxygen-containing functional group.[81] Therefore, in low-rank coal samples, the inertinite, which provides less ultra-micropores surface (compared to vitrinite), has stronger adsorption potential because the degree of polycondensation of aromatic rings of vitrinite is lower than that in inertinite. Additionally, the abundance of the functional groups of inertinite is higher than that in vitrinite. However, this phenomenon is not present in medium- and high-rank coal samples, and vitrinite evolves continuously with the deepening of metamorphism, due to which it has a greater adsorption potential.

3.5.2. Characteristics of Surface Free Energy. Figure 17 shows the reduction and rate of change of surface free energy of the samples at different pressure points. According to the changes in energy, an object always has the characteristic of achieving relative stability by reducing its energy. The same is true for coal, which can reduce its surface free energy by adsorbing methane. With the increase of pressure, the amount of adsorbed CH_4 increased, resulting in a continuous increase in the reduction of surface free energy (Figure 17a–c). Therefore, the more the reduction of surface free energy, the stronger the methane adsorption capacity of the samples, which can be represented by the descending order of $\Delta\gamma_{H1L} > \Delta\gamma_{H1M} > \Delta\gamma_{H2H}$, $\Delta\gamma_{R2L} > \Delta\gamma_{R1H} > \Delta\gamma_{R2M}$ and $\Delta\gamma_{Z1L} > \Delta\gamma_{Z1M} > \Delta\gamma_{Z2M} > \Delta\gamma_{Z2H}$.

It is seen in Figure17d–f that the rate of change of surface free energy decreases and tends to be stabilized with the increase of pressure, indicating that the influence of low pressure on surface free energy is more evident than that of high pressure. This is because the strong adsorption site of the samples is preferentially occupied by the adsorbed methane, which can reduce the surface free energy of the samples to a greater extent.[87] Furthermore, with the increase of pressure, the methane adsorption becomes more and more difficult. Therefore, the rate of change of surface free energy decreases with the increase of pressure.

From the variation pattern of the surface free energy, it is seen that the inference obtained from the low-rank coal samples is inconsistent with the CH_4 isothermal adsorption, while the results obtained from medium- and high-rank coal samples are consistent with the CH_4 isothermal adsorption. It is seen in Figure17a that the reduction of surface free energy of low-rank coal samples is much smaller than that of medium- and high-rank coal samples (the difference can be nearly 30 times). The main reason for this phenomenon is that the thermal evolution of maceral groups of low-rank coal samples is low. The pore structure is complex, and the inward force is weak, all of which lead to a smaller change in the surface free energy.

4. CONCLUSIONS

The pore structure and the thermodynamic characteristics of adsorption of different maceral groups with different ranks and particle sizes were studied. The relevant conclusions are as follows.

1. The particle size can affect the separation effect of centrifugal flotation experiments. Under the low and medium densities of $ZnCl_2$ heavy liquid, the smaller the particle size, the lower the separation of vitrinite and the higher the separation of inertinite. In the case of samples with high heavy liquid density, the optimum separation is achieved with a particle size range of 0.1–0.125 mm.
2. In the early stage of coalification, inertinite has a larger number of tissue pores than vitrinite. Therefore, inertinite can provide more pore volume and surface area in the

https://doi.org/10.1021/acsomega.2c07876
ACS Omega 2023, 8, 12079–12097

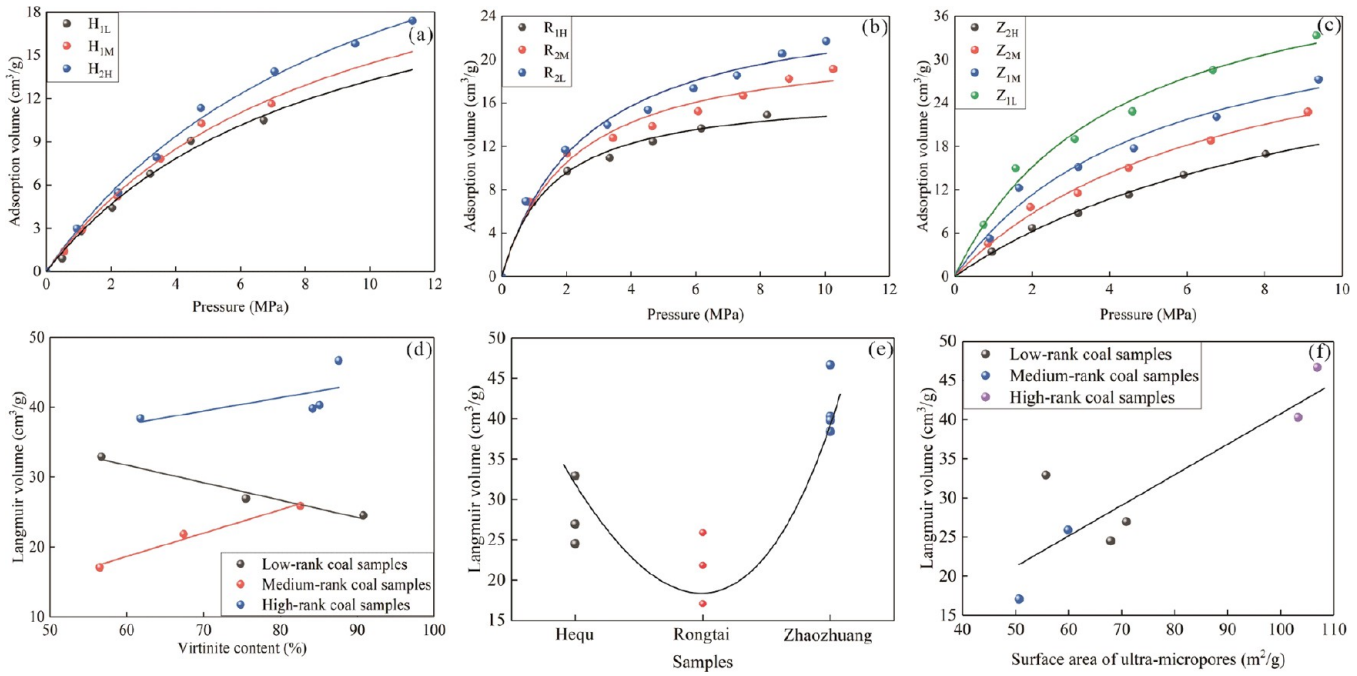

Figure 15. Characteristics of methane adsorption and Langmuir fitting (a−c: characteristics of adsorption for low-, medium-, and high-rank coal samples, respectively; d: relationship between the vitrinite content and the Langmuir volume; e: characteristics of adsorption amount of different coal ranks; f: relationship between the Langmuir volume and the surface area of ultra-micropores).

Table 5. Fitting Results for the Langmuir Volume and the Langmuir Pressure

sample	V_L (cm³/g)	P_L (MPa)	R^2
H_{1L}	24.52	8.506	0.99
H_{1M}	26.96	8.68	0.99
H_{2H}	32.94	10.04	0.99
R_{1H}	17.09	1.573	0.99
R_{2L}	25.9	2.599	0.99
R_{2M}	21.84	2.16	0.98
Z_{1L}	46.7	4.177	0.99
Z_{1M}	40.32	5.136	0.99
Z_{2M}	39.83	7.143	0.99
Z_{2H}	38.43	10.33	0.99

transition pores and mesopores (mainly within the diameter range of 40−50 nm). With the deepening of coalification, vitrinite can generate a larger number of gas pores and micropores than inertinite. Therefore, vitrinite can provide more pore volume and surface area in the ultra-micropores (mainly within the diameter range of 0.4−0.65 nm) than inertinite in the medium and high coal rank.

3. According to methane isothermal adsorption, inertinite adsorbed more methane than vitrinite in the low coal rank stages, while vitrinite adsorbed more methane than inertinite in the medium and high coal rank stages.

4. The adsorption potential, adsorption space, and surface free energy explain the adsorption characteristics of vitrinite and inertinite for methane from the point of view of thermodynamics. Based on different thermal characteristics of vitrinite and inertinite, the changes in thermodynamic parameters show that the energy changes of inertinite are greater than those of vitrinite in low-rank coal samples, whereas an opposite variation trend was observed for medium- and high-rank coal samples. The difference in energy change further clarifies the difference

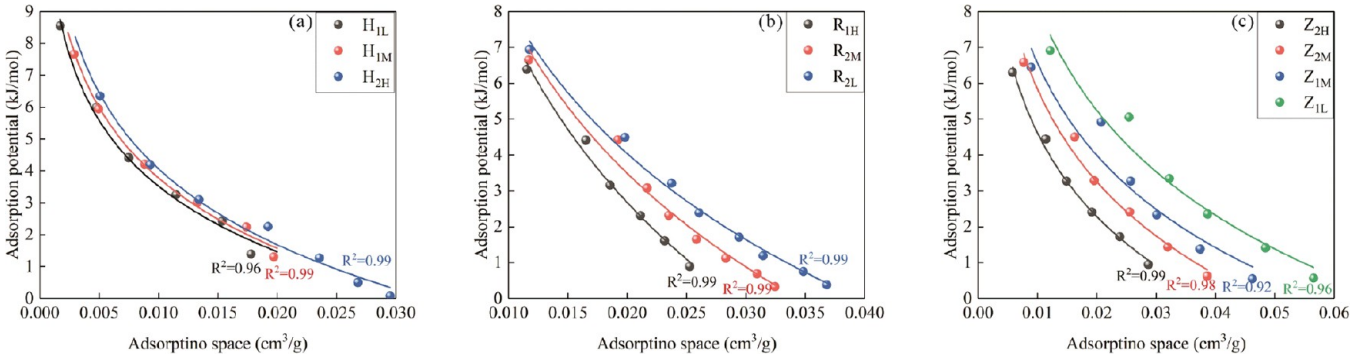

Figure 16. Characteristic curves of adsorption potential and adsorption space (a: low-rank coal samples; b: medium-rank coal samples; c: high-rank coal samples).

https://doi.org/10.1021/acsomega.2c07876
ACS Omega 2023, 8, 12079−12097

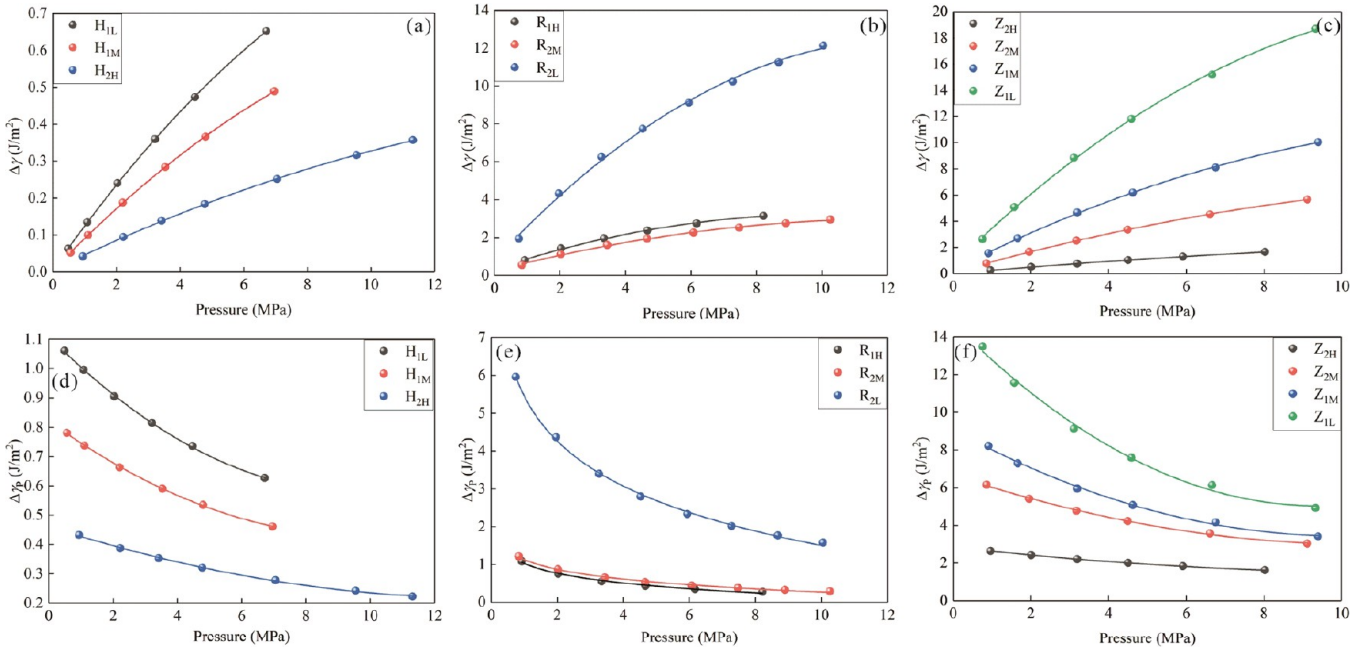

Figure 17. Reduction in the surface free energy and the rate of change of surface free energy for different coal rank samples (a−c: the reduction of surface free energy for low-, medium-, and high-rank coal samples, respectively; d−f: the rate of change of surface free energy for low-, medium-, and high-rank coal samples, respectively).

in gas adsorption capacity between the vitrinite and the inertinite.

AUTHOR INFORMATION

Corresponding Author

Songhang Zhang − *Institute of Energy Resources, Key Laboratory of Marine Reservoir Evolution and Hydrocarbon Enrichment Mechanism, Ministry of Education, and Coal Reservoir Laboratory of National Engineering Research Center of CBM Development & Utilization, China University of Geosciences, Beijing 100083, China;* orcid.org/0000-0001-6011-9108; Email: zhangsh@cugb.edu.cn

Authors

TengFei Jia − *Institute of Energy Resources, Key Laboratory of Marine Reservoir Evolution and Hydrocarbon Enrichment Mechanism, Ministry of Education, and Coal Reservoir Laboratory of National Engineering Research Center of CBM Development & Utilization, China University of Geosciences, Beijing 100083, China*

Shuheng Tang − *Institute of Energy Resources, Key Laboratory of Marine Reservoir Evolution and Hydrocarbon Enrichment Mechanism, Ministry of Education, and Coal Reservoir Laboratory of National Engineering Research Center of CBM Development & Utilization, China University of Geosciences, Beijing 100083, China*

Di Xin − *Institute of Energy Resources, Key Laboratory of Marine Reservoir Evolution and Hydrocarbon Enrichment Mechanism, Ministry of Education, and Coal Reservoir Laboratory of National Engineering Research Center of CBM Development & Utilization, China University of Geosciences, Beijing 100083, China*

Qian Zhang − *Institute of Energy Resources, Key Laboratory of Marine Reservoir Evolution and Hydrocarbon Enrichment Mechanism, Ministry of Education, and Coal Reservoir Laboratory of National Engineering Research Center of CBM Development & Utilization, China University of Geosciences, Beijing 100083, China*

Ke Zhang − *Institute of Energy Resources, Key Laboratory of Marine Reservoir Evolution and Hydrocarbon Enrichment Mechanism, Ministry of Education, and Coal Reservoir Laboratory of National Engineering Research Center of CBM Development & Utilization, China University of Geosciences, Beijing 100083, China*

Complete contact information is available at: https://pubs.acs.org/10.1021/acsomega.2c07876

Notes

The authors declare no competing financial interest.

ACKNOWLEDGMENTS

This research is funded by the National Natural Science Foundation of China (Nos. 41872178 and U1910205).

REFERENCES

(1) Refaat, T. F.; Ismail, S.; Nehrir, A. R.; Hair, J. W.; Crawford, J. H.; Leifer, I.; Shuman, T. Performance evaluation of a 1.6-mu m methane DIAL system from ground, aircraft and UAV platforms. *Opt. Express* **2013**, *21*, 30415−30432.

(2) Yang, J.; Urpelainen, J. Is coal-fired power generation associated with rural electrification?A global analysis. *Energy Res. Soc. Sci.* **2019**, *58*, No. 101274.

(3) Vishal, V.; Chandra, D.; Singh, U.; Verma, Y. Understanding initial opportunities and key challenges for CCUS deployment in India at scale. *Ress Conserv.Recycl.* **2021**, *175*, No. 105829.

(4) Mohanty, M. M.; Pal, B. K. Sorption behavior of coal for implication in coal bed methane an overview. *Int. J. Mining Sci. Technol.* **2017**, *27*, 307−314.

(5) Zhang, Z.; Huisingh, D. Carbon dioxide storage schemes: Technology, assessment and deployment. *J. Cleaner Prod.* **2017**, *142*, 1055−1064.

(6) Jia, Z.; Lin, B. How to achieve the first step of the carbon-neutrality 2060 target in China: The coal substitution perspective. *Energy* **2021**, *233*, No. 121179.
(7) Detheridge, A.; Hosking, L. J.; Thomas, H. R.; Sarhosis, V.; Gwynn-Jones, D.; Scullion, J. Deep seam and minesoil carbon sequestration potential of the South Wales Coalfield, UK. *J. Environ. Manage.* **2019**, *248*, No. 109325.
(8) Xu, H. J.; Sang, S. X.; Yang, J. F.; Liu, H. H. CO_2 storage capacity of anthracite coal in deep burial depth conditions and its potential uncertainty analysis: a case study of the No.3 coal seam in the Zhengzhuang Block in Qinshui Basin, China. *Geosci. J.* **2021**, *25*, 715−729.
(9) Chen, M.; Lu, Y.; Kang, Y.; You, L.; Chen, Z.; Liu, J.; Li, P. Investigation of enhancing multi-gas transport ability of coalbed methane reservoir by oxidation treatment. *Fuel* **2020**, *278*, No. 118377.
(10) Verma, S.; Chaudhari, S. Highlights from the literature on risk assessment techniques adopted in the mining industry: A review of past contributions, recent developments and future scope. *Int. J. Mining Sci. Technol.* **2016**, *26*, 691−702.
(11) Pan, Z.; Wood, D. A. Coalbed methane (CBM) exploration, reservoir characterisation, production, and modelling: A collection of published research (2009-2015). *J. Nat. Gas Sci. Eng.* **2015**, *26*, 1472−1484.
(12) Gabrus, E.; Wojtacha-Rychter, K.; Aleksandrzak, T.; Smolinski, A.; Krol, M. The feasibility of CO_2 emission reduction by adsorptive storage on Polish hard coals in the Upper Silesia Coal Basin: An experimental and modeling study of equilibrium, kinetics and thermodynamics. *Sci. Total Environ.* **2021**, *796*, No. 149064.
(13) Tarkowski, R.; Czapowski, G. Salt domes in Poland - Potential sites for hydrogen storage in caverns. *Int. J. Hydrogen Energy* **2018**, *43*, 21414−21427.
(14) Fan, W.; Chakraborty, A.; Kayal, S. Adsorption cooling cycles: Insights into carbon dioxide adsorption on activated carbons. *Energy* **2016**, *102*, 491−501.
(15) Rodrigues, C. F.; de Sousa, M. J. L. The measurement of coal porosity with different gases. *Int. J. Coal Geol.* **2002**, *48*, 245−251.
(16) Wei, Y. C.; Li, C.; Cao, D. Y.; Wang, A. M.; Zhang, A. X.; Yao, Z. The effects of particle size and inorganic mineral content on fines migration in fracturing proppant during coalbed methane production. *J. Pet. Sci. Eng.* **2019**, *182*, No. 106355.
(17) Teng, J.; Mastalerz, M.; Hampton, L. Maceral controls on porosity characteristics of lithotypes of Pennsylvanian high volatile bituminous coal: Example from the Illinois Basin. *Int. J. Coal Geol.* **2017**, *172*, 80−94.
(18) Lin, Y.; Qin, Y.; Ma, D.; Duan, Z. Pore structure, adsorptivity and influencing factors of high-volatile bituminous coal rich in inertinite. *Fuel* **2021**, *293*, No. 120418.
(19) Zhang, S.; Liu, H.; Wu, C.; Jin, Z. Influence of particle size on pore structure and multifractal characteristics in coal using low-pressure gas adsorption. *J. Pet.Sci. Eng.* **2022**, *212*, No. 110273.
(20) Liu, L. T.; Jin, C.; Li, L.; Xu, C. Y.; Sun, P. F.; Meng, Z. X.; An, L. L. Coalbed methane adsorption capacity related to maceral compositions. *Energy Explor. Exploit.* **2020**, *38*, 79−91.
(21) Gensterblum, Y.; Merkel, A.; Busch, A.; Krooss, B. M.; Littke, R. Gas saturation and CO_2 enhancement potential of coalbed methane reservoirs as a function of depth. *AAPG Bulletin* **2014**, *98*, 395−420.
(22) Zhao, J.; Xu, H.; Tang, D.; Mathews, J. P.; Li, S.; Tao, S. A comparative evaluation of coal specific surface area by CO_2 and N_2 adsorption and its influence on CH_4 adsorption capacity at different pore sizes. *Fuel* **2016**, *183*, 420−431.
(23) Das, P. R.; Mendhe, V. A.; Kamble, A. D.; Sharma, P.; Shukla, P.; Varma, A. K. Petrographic and Geochemical Controls on Methane Genesis, Pore Fractal Attributes, and Sorption of Lower Gondwana Coal of Jharia Basin. *India. ACS Omega* **2022**, *7*, 299−324.
(24) Czerw, Y.; Dudzinska, A.; Baran, P.; Zarebska, K. Sorption of carbon dioxide on the lithotypes of low rank coal. *Adsorp.-J. Int. Adsorp. Soc.* **2019**, *25*, 965−972.
(25) Hou, H.; Shao, L.; Li, Y.; Li, Z.; Wang, S.; Zhang, W.; Wang, X. Influence of coal petrology on methane adsorption capacity of the Middle Jurassic coal in the Yugia Coalfield, northern Qaidam Basin, China. *J. Pet.Sci. Eng.* **2017**, *149*, 218−227.
(26) Weishauptova, Z.; Pribyl, O.; Sykorova, I.; Machovic, V. Effect of bituminous coal properties on carbon dioxide and methane high pressure sorption. *Fuel* **2015**, *139*, 115−124.
(27) Weishauptova, Z.; Sykorova, I. Dependence of carbon dioxide sorption on the petrographic composition of bituminous coals from the Czech part of the Upper Silesian Basin, Czech Republic. *Fuel* **2011**, *90*, 312−323.
(28) Chalmers, G. R. L.; Bustin, R. M. On the effects of petrographic composition on coalbed methane sorption. *Int. J. Coal Geol.* **2007**, *69*, 288−304.
(29) Mastalerz, M.; Gluskoter, H.; Rupp, J. Carbon dioxide and methane sorption in high volatile bituminous coals from Indiana, USA. *Int. J. Coal Geol.* **2004**, *60*, 43−55.
(30) Zhang, H.; Zhang, X. B.; Zhang, Y. G.; Lei, D. J. Acidic oxygen-containing groups and their inhibition methane adsorption of Yima lignite maceral components. *J. China Univ. Min. Technol.* **2018**, *47*, 1149−1156.
(31) Yang, F.; Ma, D.; Duan, Z.; Ren, D.; Tian, T.; Fu, D. Micropore Structural Characteristics and Influence Factors of Triassic Shale Gas Adsorption in the Ordos Basin. *Front. Phys.* **2022**, *10*, No. 851131.
(32) Yao, Y. B.; Liu, D. M. Adsorption Characteristics of Coal Reservoirs in North China and Its Influencing Factors. *J. China Univ. Min. Technol.* **2007**, *36*, 308−314.
(33) Zhang, L. P.; Su, X. B.; Zeng, R. S. Discussion on the Controlling Effects of Coal Properties on Coal Adsorption Capacity. *Acta Geol. Sin.* **2006**, *80*, 910−915.
(34) Kiani, A.; Sakurovs, R.; Grigore, M.; Sokolova, A. Gas sorption capacity, gas sorption rates and nanoporosity in coals. *Int. J. Coal Geol.* **2018**, *200*, 77−86.
(35) Shan, C. A.; Zhang, T. S.; Liang, X.; Zhang, Z.; Zhu, H. H.; Yang, W.; Zhang, K. Influence of chemical properties on CH_4 adsorption capacity of anthracite derived from southern Sichuan Basin, China. *Mar. Pet. Geol.* **2018**, *89*, 387−401.
(36) Weniger, P.; Kalkreuth, W.; Busch, A.; Krooss, B. M. High-pressure methane and carbon dioxide sorption on coal and shale samples from the Parana Basin, Brazil. *Int. J. Coal Geol.* **2010**, *84*, 190−205.
(37) Chalmers, G. R. L.; Bustin, R. M. Lower Cretaceous gas shales in northeastern British Columbia, Part I: geological controls on methane sorption capacity. *Bull. Can. Pet. Geol.* **2008**, *56*, 1−21.
(38) Clarkson, C. R.; Bustin, R. M. Binary gas adsorption/desorption isotherms: effect of moisture and coal composition upon carbon dioxide selectivity over methane. *Int. J. Coal Geol.* **2000**, *42*, 241−271.
(39) Mendhe, V. A.; Kamble, A. D.; Bannerjee, M.; Mishra, S.; Mukherjee, S.; Mishra, P. Evaluation of shale gas reservoir in Barakar and barren measures formations of north and south Karanpura Coalfields. Jharkhand. *J. Geol. Soc. India* **2016**, *88*, 305−316.
(40) Yuan, J. H.; Zhang, H.; Guo, Y. L.; Cai, N. Thermodynamic properties of high-rank tectonically deformed coals during isothermal adsorption. *Arab. J. Geosci.* **2017**, *10*, 278.
(41) Shan, C. A.; Zhang, T. S.; Liang, X.; Hu, R. R.; Zhao, W. W. Nanopore structure characteristics of high-rank vitrinite-and inertinite-coal. *Acta Pet. Sin.* **2020**, *41*, 723−736.
(42) Zhang, M.; Fu, X. H. Characterization of pore structure and its impact on methane adsorption capacity for semi-anthracite in Shizhuangnan Block, Qinshui Basin. *J. Nat. Gas Sci. Eng.* **2018**, *60*, 49−62.
(43) Zhao, W.; Wang, K.; Liu, S. M.; Ju, Y.; Zhou, H. W.; Fan, L.; Yang, Y.; Cheng, Y. P.; Zhang, X. L. Asynchronous difference in dynamic characteristics of adsorption swelling and mechanical compression of coal: Modeling and experiments. *Int. J. Rock Mech. Mining Sci.* **2020**, *135*, No. 104498.
(44) Wu, S.; Tang, D. Z.; Li, S.; Chen, H.; Wu, H. Y. Coalbed methane adsorption behavior and its energy variation features under supercritical pressure and temperature conditions. *J. Pet.Sci. Eng.* **2016**, *146*, 726−734.

https://doi.org/10.1021/acsomega.2c07876
ACS Omega 2023, 8, 12079−12097

(45) Meng, Z.; Liu, S.; Li, G. Adsorption capacity, adsorption potential and surface free energy of different structure high rank coals. *J. Pet.Sci. Eng.* **2016**, *146*, 856−865.
(46) Du, X. D.; Cheng, Y. G.; Liu, Z. J.; Yin, H.; Wu, T. F.; Huo, L.; Shu, C. X. CO_2 and CH_4 adsorption on different rank coals: A thermodynamics study of surface potential, Gibbs free energy change and entropy loss. *Fuel* **2021**, *283*, No. 118886.
(47) Ye, J. C.; Tao, S.; Zhao, S. P.; Li, S.; Chen, S. D.; Cui, Y. Characteristics of methane adsorption/desorption heat and energy with respect to coal rank. *J. Nat. Gas Sci. Eng.* **2022**, *99*, No. 104445.
(48) Liu, D.; Zou, Z.; Cai, Y.; Qiu, Y.; Zhou, Y.; He, S. An updated study on CH_4 isothermal adsorption and isosteric adsorption heat behaviors of variable rank coals. *J. Nat. Gas Sci. Eng.* **2021**, *89*, No. 103899.
(49) Qiu, F.; Liu, D.; Cai, Y.; Liu, N.; Qiu, Y. Methane Adsorption Interpreting with Adsorption Potential and Its Controlling Factors in Various Rank Coals. *Processes* **2020**, *8*, 390.
(50) Lu, G. W.; Wei, C. T.; Wang, J. L.; Meng, R. Y.; Tamehe, L. S. Influence of pore structure and surface free energy on the contents of adsorbed and free methane in tectonically deformed coal. *Fuel* **2021**, *285*, No. 119087.
(51) Zhang, J.; Wei, C.; Zhao, C.; Zhang, T.; Lu, G.; Zou, M. Effects of nano-pore and macromolecule structure of coal samples on energy parameters variation during methane adsorption under different temperature and pressure. *Fuel* **2021**, *289*, No. 119804.
(52) Bahrami, A.; Jamialahmadi, M.; Moghadasi, J.; Alimohammadi, N. Simulation study of CO_2 sequestration potential of the Mary Lee coal zone, Black Warrior basin. *Environ. Earth Sci.* **2013**, *70*, 2501−2509.
(53) Hao, S. X.; Chu, W.; Jiang, Q.; Yu, X. P. Methane adsorption characteristics on coal surface above critical temperature through Dubinin-Astakhov model and Langmuir model. *Colloids Surf., A* **2014**, *444*, 104−113.
(54) Xin, D.; Tang, S. H.; Zhang, S. H.; Xi, Z. D. Declining High-Pressure Sorption Isotherms on Shale and Coal: Systematic Comparison of the Contributing Factors. *Energy Fuels* **2021**, *35*, 15695−15708.
(55) Polanyi, M. The Potential Theory of Adsorption. *Science* **1963**, *141*, 1010−1013.
(56) Ramirez-Pastor, A. J.; Bulnes, F. Differential heat of adsorption in the presence of an order-disorder phase transition. *Phys. A* **2000**, *283*, 198−203.
(57) Lu, G.; Wei, C.; Wang, J.; Zhang, J.; Quan, F.; Tamehe, L. Variation of Surface Free Energy in the Process of Methane Adsorption in the Nanopores of Tectonically Deformed Coals: A Case Study of Middle-Rank Tectonically Deformed Coals in the Huaibei Coalfield. *Energy Fuels* **2019**, *33*, 7155−7165.
(58) Amankwah, K. A. G.; Schwarz, J. A. A modified approach for estimating pseudo-vapor pressures in the application of the dubinin-astakhov equation. *Carbon* **1995**, *33*, 1313−1319.
(59) Loh, W. S.; Rahman, K. A.; Chakraborty, A.; Saha, B. B.; Choo, Y. S.; Khoo, B. C.; Ng, K. C. Improved Isotherm Data for Adsorption of Methane on Activated Carbons. *J. Chem. Eng. Data* **2010**, *55*, 2840−2847.
(60) Dyrkacz, G. R.; Bloomquist, C. A. A.; Ruscic, L. Chemical variations in coal macerals separated by density gradient centrifugation. *Fuel* **1984**, *63*, 1166−1173.
(61) Liu, Y.; Kang, J.; Zhou, F.; Fan, Y.; Li, H. Effects of Maceral Compositions of Coal on Methane Adsorption Heat. *Geofluids* **2018**, 1.
(62) Hou, S.; Wang, X.; Wang, X.; Yuan, Y.; Pan, S.; Wang, X. Pore structure characterization of low volatile bituminous coals with different particle size and tectonic deformation using low pressure gas adsorption. *Int. J. Coal Geol.* **2017**, *183*, 1−13.
(63) Brunauer, S.; Deming, L. S.; Deming, W. E.; Teller, E. On a Theory of the van der Waals Adsorption of Gases. *J. Am. Chem. Soc.* **1940**, *62*, 1723−1732.
(64) Jia, T.; Zhang, S.; Tang, S.; Wang, M.; Xin, D.; Zhang, Q. Characteristics and Evolution of Low-Rank Coal Pore Structure Around the First Coalification Jump: Case Study in Southeastern Junggar Basin. *Nat. Resour. Res.* **2022**, *31*, 2769−2786.
(65) Thommes, M.; Kaneko, K.; Neimark, A. V.; Olivier, J. P.; Rodriguez-Reinoso, F.; Rouquerol, J.; Sing, K. S. W. Physisorption of gases, with special reference to the evaluation of surface area and pore size distribution (IUPAC Technical Report). *Pure Appl. Chem.* **2015**, *87*, 1051−1069.
(66) Vranjes-Wessely, S.; Misch, D.; Issa, I.; Kiener, D.; Fin, K. R.; Seemann, T.; Liu, B.; Rantitsch, G.; Sachsenhofer, R. F. Nanoscale pore structure of Carboniferous coals from the Ukrainian Donets Basin: A combined HRTEM and gas sorption study. *Int. J. Coal Geol.* **2020**, *224*, No. 103484.
(67) Wang, Z.; Cheng, Y.; Wang, G.; Ni, G.; Wang, L. Comparative analysis of pore structure parameters of coal by using low pressure argon and nitrogen adsorption. *Fuel* **2022b**, *309*, No. 122120.
(68) Bertier, P.; Schweinar, K.; Stanjek, H.; Ghanizadeh, A.; Pipich, V. J. C. W. L. On the use and abuse of N_2 physisorption for the characterisation of the pore structure of shales. *CMS Workshop Lectures* **2016**, *21*, 151−161.
(69) Louw, E. B.; Mitchell, G. D.; Wang, J.; Winans, R. E.; Mathews, J. P. Constitution of Drop-Tube-Generated Coal Chars from Vitrinite- and Inertinite-Rich South African Coals. *Energy Fuels* **2016**, *30*, 112−120.
(70) Teichmüller, M. The genesis of coal from the viewpoint of coal petrology. *Int. J. Coal Geol.* **1989**, *12*, 1−87.
(71) Wang, A.; Cao, D.; Wei, Y.; Nie, J.; Qin, R. Comparison of nanopore evolution in vitrinite and inertinite in coalbed methane reservoirs during coalification. *J. Nat. Gas Sci. Eng.* **2020**, *78*, No. 103289.
(72) He, X.; Sun, H.; Ma, M.; Zhang, X.; Wang, W. Enrichment Characteristics of Macerals during Triboelectrostatic Separation in the View of Surface Microstructure, Pore distribution, and Typical Electrical Parameters. *ACS Omega* **2021**, *6*, 18509−18517.
(73) Mastalerz, M.; Hampton, L.; Drobniak, A.; Loope, H. Significance of analytical particle size in low-pressure N_2 and CO_2 adsorption of coal and shale. *Int. J. Coal Geol.* **2017**, *178*, 122−131.
(74) Wang, Z.; Cheng, Y.; Qi, Y.; Wang, R.; Wang, L.; Jiang, J. Experimental study of pore structure and fractal characteristics of pulverized intact coal and tectonic coal by low temperature nitrogen adsorption. *Powder Technol.* **2019**, *350*, 15−25.
(75) Zhang, B.; Chen, Y. Particle size effect on pore structure characteristics of lignite determined via low-temperature nitrogen adsorption. *J. Nat. Gas Sci. Eng.* **2020**, *84*, No. 103633.
(76) Hou, C.; Jiang, B.; Liu, H.; Song, Y.; Xu, S. The differences of nanoscale mechanical properties among coal maceral groups. *J. Nat. Gas Sci. Eng.* **2020**, *80*, No. 103394.
(77) Chen, Y.; Wei, L.; Mastalerz, M.; Schimmelmann, A. The effect of analytical particle size on gas adsorption porosimetry of shale. *Int. J. Coal Geol.* **2015**, *138*, 103−112.
(78) Shu, Y.; Xu, Y.; Jiang, S.; Zhang, L.; Zhao, X.; Pan, Z.; Blach, T.; Sun, L.; Bai, L.; Hu, Q.; Sun, M. Effect of Particle Size on Pore Characteristics of Organic-Rich Shales: Investigations from Small-Angle Neutron Scattering (SANS) and Fluid Intrusion Techniques. *Energies* **2020**, *13*, 6049.
(79) Wang, L.; Long, Z.; Song, Y.; Qu, Z. Supercritical CO_2 adsorption and desorption characteristics and pore structure controlling mechanism of tectonically deformed coals. *Fuel* **2022a**, *317*, No. 123485.
(80) Li, X.; Chen, X.; Zhang, F.; Zhang, M.; Zhang, Q.; Jia, S. Energy Calculation and Simulation of Methane Adsorbed by Coal with Different Metamorphic Grades. *ACS Omega* **2020**, *5*, 14976−14989.
(81) Meng, J.; Niu, J.; Meng, H.; Xia, J.; Zhong, R. Insight on adsorption mechanism of coal molecules at different ranks. *Fuel* **2020**, *267*, No. 117234.
(82) Zhou, H.; Wu, C.; Pan, J.; Wang, Z.; Niu, Q.; Du, M. Research on Molecular Structure Characteristics of Vitrinite and Inertinite from Bituminous Coal with FTIR, Micro-Raman, and XRD Spectroscopy. *Energy Fuels* **2021**, *35*, 1322−1335.

https://doi.org/10.1021/acsomega.2c07876
ACS Omega 2023, 8, 12079−12097

(83) Mastalerz, M.; Bustin, R. M. Variation in maceral chemistry within and between coals of varying rank: An electron microprobe and micro-Fourier transform infra-red investigation. *J. Microsc.-Oxford* **1993**, *171*, 153−166.
(84) He, X.; Liu, X.; Nie, B.; Song, D. FTIR and Raman spectroscopy characterization of functional groups in various rank coals. *Fuel* **2017**, *206*, 555−563.
(85) Li, Y. X.; Wu, S. Y.; Li, C. L.; Zhang, M. H. Analysis on Applicability of Different Adsorption Model Based on the Molecular Inter-Atomic Forces. *Chin. J. Tunn. Undergr. Space Eng.* **2014**, *10*, 1121−1126.
(86) Mosher, K.; He, J. J.; Liu, Y. Y.; Rupp, E.; Wilcox, J. Molecular simulation of methane adsorption in micro- and mesoporous carbons with applications to coal and gas shale systems. *Int. J. Coal Geol.* **2013**, *109*, 36−44.
(87) Li, F.; Jiang, B.; Cheng, G.; Song, Y. Methane Adsorption Behavior and Energy Variations of Brittle Tectonically Deformed Coal under High Temperature and High Pressure. *ACS Omega* **2022**, *7*, 2737−2751.

https://doi.org/10.1021/acsomega.2c07876
ACS Omega 2023, 8, 12079−12097